J|A|C|S
ARTICLES
Published on Web 02/22/2002

Density Functional Calculations of Electronic g-Tensors for Semiquinone Radical Anions. The Role of Hydrogen Bonding and Substituent Effects

Martin Kaupp,*,† Christian Remenyi,† Juha Vaara,‡ Olga L. Malkina,§,|| and Vladimir G. Malkin||

Contribution from the Institut für Anorganische Chemie, Universität Würzburg, Am Hubland, D-97074 Würzburg, Germany, Department of Chemistry, P.O. Box 55 (A.I. Virtasen aukio 1), FIN-00014, University of Helsinki, Finland, Computing Center, Slovak Academy of Sciences, Dubravska Cesta 9, SK-84236 Bratislava, Slovakia, and Institute of Inorganic Chemistry, Slovak Academy of Sciences, Dubravska Cesta 9, SK-84236 Bratislava, Slovakia

Received May 25, 2001. Revised Manuscript Received November 5, 2001

Abstract: A recently developed density functional approach has been used to carry out a systematic computational study of electronic **g**-tensors for a series of 1,4-semiquinone radical anions. Good agreement with high-field EPR data in frozen 2-propanol is achieved only after taking into account the significant reduction of **g**-tensor anisotropy caused by hydrogen bonding to solvent molecules. The comparison of various model systems for the first solvation shell suggests two hydrogen bonds from 2-propanol molecules to each of the carbonyl groups of the radical anions, and one additional hydrogen bond to each of the methoxy groups in ubiquinone systems. 2-Propanol makes stronger hydrogen bonds than water and thus influences **g**-tensor anisotropy more strongly. Substituent effects at the semiquinone are reproduced quantitatively by the calculations. The **g**-tensor anisotropy is influenced significantly by the conformations of methyl and methoxy substituents, with opposite contributions. Analyses and interpretations of the interrelations between structure, bonding, and spectroscopic data are provided. The relevance of the computational results for the EPR spectroscopy of semiquinone radical anions in photosynthetic reaction centers is discussed.

1. Introduction

Quinones (Q) are central to several of the most important processes of life, such as respiration and photosynthesis.[1] On the way to chemical, electrochemical, or photochemical reduction of quinones (eventually to hydroquinones QH_2), semiquinones are formed as intermediates, either in the form of the radical anions $Q^{\bullet -}$ or in the monoprotonated form $QH^{\bullet}$. Due to the important role of such radical species, e.g., in the primary electron-transfer step of photosynthesis, a vast number of electron paramagnetic resonance (EPR) studies have been carried out on semiquinone radical anions, both in their biological surroundings and in isotropic (frozen or liquid) solution.[2−15] The development of high-field EPR spectroscopy during the past decade has added significantly to the progress in this field. Specifically, solid-state experiments at high magnetic fields have allowed for the first time the accurate determination of the electronic **g**-tensors of organic radicals.[5,6,8−12,14,15]

There are strong indications that the **g**-tensor of semiquinone radical anions depends significantly on the presence or absence of hydrogen bonding.[2,3,6,14−18] In particular, it appears that strong hydrogen bonding to the carbonyl oxygen atoms of the radical anions reduces the **g**-tensor anisotropy noticeably, thus providing a direct probe of the strength of hydrogen bonding in the specific protein environment. For example, significantly larger g_{xx} components of the **g**-tensors (i.e., the components oriented parallel to the carbonyl C−O bonds) have been found for semiquinone radicals in photosystem I (PS−I) of higher organisms compared to those in bacterial reaction centers (bRC) or those in photosystem II (PS−II).[9−12] These differences have been attributed to less pronounced hydrogen bonding to the semiquinone in PS−I.

* To whom correspondence should be addressed. E-mail: kaupp@mail.uni-wuerzburg.de.
† Universität Würzburg.
‡ University of Helsinki.
§ Computing Center.
|| Institute of Inorganic Chemistry.

(1) Patai, S. *Chemistry of Quinoid Compounds*; Interscience: New York 1974. Trumpower, B. L., Ed. *Function of Quinones in Energy Conserving Systems*; Academic Press: New York, 1982. Morton, R. A. *Biochemistry of Quinones*; Academic Press: New York, 1965.
(2) Hales, B. J. *J. Am. Chem. Soc.* **1975**, *97*, 5993.
(3) Pedersen, J. A. *EPR Spectra from Natural and Synthetic Quinones and Quinoids*; CRC Press: Boca Raton, FL, 1985.
(4) See, e.g., (a) O'Malley, P. J.; Babcock, G. T. *J. Chem. Phys.* **1984**, *80*, 3912. (b) O'Malley, P. J.; Babcock, G. T. *J. Am. Chem. Soc.* **1986**, *108*, 3995. (c) Lubitz, W.; Abresch, E. C.; Debus, R. J.; Isaacson, R. A.; Okamura, M. Y.; Feher, G. *Biochim. Biophys. Acta* **1985**, *808*, 464. (d) Niethammer, D.; Kirste, B.; Kurreck, H. *J. Chem. Soc., Faraday Trans.* **1990**, *86*, 3191. (e) Samoilova, R. I.; van Liemt, W.; Steggerda, W. F.; Lugtenburg, J.; Hoff, A. J.; Spoyalov, A. P.; Tyryshkin, A. M.; Gritzan, N. P.; Tsvetkov, Y. D. *J. Chem. Soc., Perkin Trans. 2* **1994**, 609. (f) Samoilova, R. I.; Gritsan, N. P.; Hoff, A. J.; van Liemt, W.; Lugtenburg, J.; Spoyalov, A. P.; Tsvetkov, Y. D. *J. Chem. Soc., Perkin Trans. 2* **1995**, 2063. (g) van den Brink; J. S.; Spoyalov, A. P.; Gastl, P.; van Liemt, W. B. S.; Raap, J.; Lugtenburg, J.; Hoff, A. J. *FEBS Lett.* **1994**, *353*, 273. (g) van den Brink; J. S.; Hulsebosch, R. J.; Gastl, P.; Hore, P. J.; Hoff, A. J. *Biochemistry* **1994**, *33*, 13668.

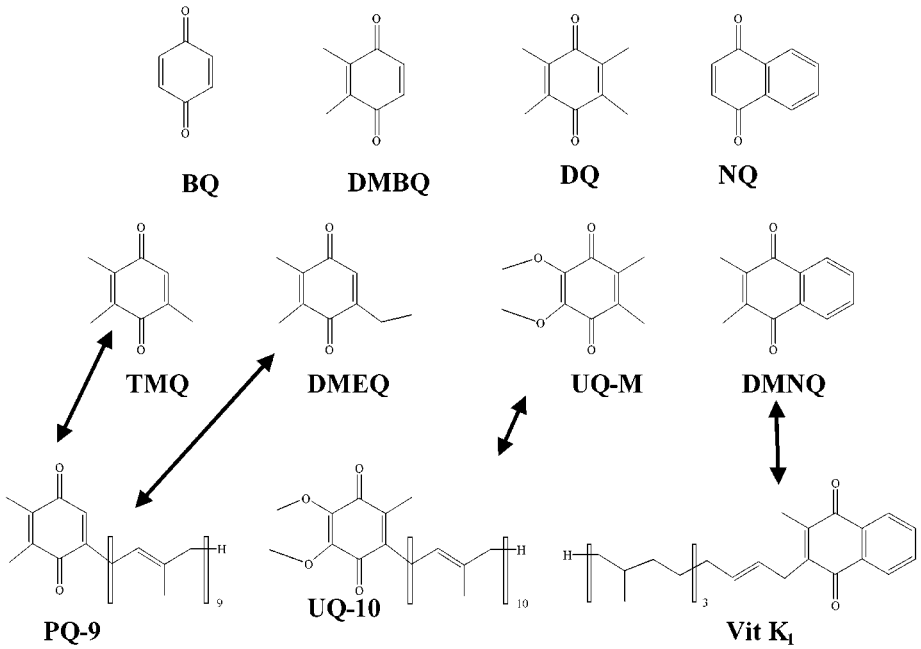

Figure 1. 1,4-Quinone systems, from which the semiquinone radical anions studied in this work derive. Arrows indicate the function of molecules with shortened side chains as models for biologically relevant quinones. The following abbreviations have been used: BQ (1,4-benzoquinone), DMBQ (2,3-dimethyl-1,4-benzoquinone), DMEQ (2,3-dimethyl-5-ethyl-1,4-benzoquinone, studied as model for plastoquinone-9), DQ (duroquinone: 2,3,5,6-tetramethyl-1,4-benzoquinone), TMQ (2,3,5-trimethyl-1,4-benzoquinone, studied as model for plastoquinone-9), UQ-M (2,3-dimethoxy-5,6-dimethyl-1,4-benzoquinone, studied as model for ubiquinone-10), NQ (1,4-naphthoquinone), DMNQ (2,3-dimethyl-1,4-naphthoquinone, studied as model for vitamin K_1). The last row of the figure shows three related, biologically relevant quinones: PQ-9 (plastoquinone-9: 2,3-dimethyl-5-solanesyl-1,4-benzoquinone), UQ-10 (ubiquinone-10: 2,3-dimethoxy-5-methyl-6-decaprenyl-1,4-benzoquinone), Vit-K_1 (vitamin K_1, phylloquinone: 2-methyl-3-phytyl-1,4-naphthoquinone).

The interpretation of the **g**-tensors, and thus the elucidation of the protein environment of the quinones/semiquinones, should benefit greatly from quantum chemical calculations. Except for a recent MCSCF calculation of the **g**-tensor for the free benzosemiquinone radical anion,[19] previous theoretical studies have been restricted to rather approximate semiempirical methods.[2,6,16,20−23] While these have provided many important qualitative insights, e.g., into the influence of hydrogen bonding on the **g**-tensors, quantitative predictions have not been possible. Here we report the first systematic first-principles theoretical study of electronic **g**-tensors for a variety of 1,4-semiquinone radical anions. We employ a recently developed density functional method for the calculation of **g**-tensors.[24] The electronic **g**-tensor is strongly dependent on spin−orbit coupling. Therefore, computationally efficient yet particularly accurate approximations to the full molecular one- and two-electron spin−orbit operators are a main feature of our approach. This allows for the first time to exploit fully the accuracy of the underlying density functional methodology. We study the radical anions of a series of differently substituted quinones (Figure 1), including appropriate model systems for those quinones present in photosynthetic reaction centers. The important

(5) See, e.g., Yang, F.; Shen, G.; Schluchter, W. M.; Zybailov, B.; Ganago, A. O.; Vassiliev, I. R.; Bryant, D. A.; Golbeck, J. H. *J. Phys. Chem. B* **1998**, *102*, 8288. Kamlowski, A.; Zech, S. G.; Fromme, P.; Bittl, R.; Lubitz, W.; Witt, H. T.; Stehlik, D. *J. Phys. Chem. B* **1998**, *102*, 8266. Rohrer, M.; MacMillan, F.; Prisner, T. F.; Gardiner, A. T.; Möbius, K.; Lubitz, W. *J. Phys. Chem. B* **1998**, *102*, 4648. Calvo, R.; Abresch, E. C.; Bittl, R.; Feher, G.; Hofbauer, W.; Isaacson, R. A.; Lubitz, W.; Okamura, M. Y.; Paddock, M. L. *J. Am. Chem. Soc.* **2000**, *122*, 7327. Calvo, R.; Isaacson, R. A.; Paddock, M. L. Abresch, E. C.; Okamura, M. Y.; Maniero, A.-L.; Brunel, L.-C.; Feher, G. *J. Phys. Chem. B* **2001**, *105*, 4053. Rigby, E. E. J.; Evans, M. C. W.; Heathcote, P. *Biochemistry* **1996**, *35*, 6651. Prisner, T. F.; van der Est, A.; Bittl, R.; Lubitz, W.; Stehlik, D.; Möbius, K. *Chem. Phys.* **1995**, *194*, 361. Zech, S. G.; Kurreck, J.; Renger, G.; Lubitz, W.; Bittl, R. *FEBS Lett.* **1999**, *442*, 79. Füchsle, G.; Bittl, R.; van der Est, A.; Lubitz, W.; Stehlik, D. *Biochim. Biophys. Acta* **1993**, *1142*, 23. Deligiannakis, Y.; Boussac, A.; Rutherford, A. W. *Biochemistry* **1995**, *34*, 16030. Link, G.; Berthold, M.; Weidner, J.-U.; Ohmes, E.; Tang, J.; Poluekto'v, O.; Utschig, L.; Schlesselman, S. L.; Thurnauer, M. C.; Kothe, G. *J. Am. Chem. Soc.* **2001**, *123*, 4211. Hanley, J.; Deligiannakis, Y.; MacMillan, F.; Bottin, H.; Rutherford, W. A. *Biochemistry* **1997**, *36*, 11543. Ostafin, A. E.; Weber, S. *Biochim. Biophys. Acta* **1997**, *1320*, 195. Bittl, R.; Zech, S. G.; Fromme, P.; Witt, H. T.; Lubitz, W. *Biochemistry* **1997**, *36*, 12001. Bittl, R.; Zech, S. G. *J. Phys. Chem. B* **1997**, *101*, 1429.
(6) Burghaus, O.; Plato, M.; Rohrer, M.; Möbius, K.; MacMillan, F.; Lubitz, W. *J. Phys. Chem.* **1993**, *97*, 7639. Rohrer, M. Plato, M.; MacMillan, F.; Grishin, Y.; Lubitz, W.; Möbius, K. *J. Magn. Reson.* **1995**, *116*, 59.
(7) Nimz, O.; Lendzian, F.; Boullais, C.; Lubitz, W. *Appl. Magn. Reson.* **1998**, *14*, 255.
(8) MacMillan, F.; Lendzian, F.; Lubitz, W. *Magn. Reson. Chem.* **1995**, *33*, 81.
(9) van der Est, A.; Sieckmann, I.; Lubitz, W.; Stehlik, D. *Chem. Phys.* **1995**, *194*, 349.
(10) Kamlowski, A.; Altenberg-Greulich, B.; van der Est, A.; Zech, S. G.; Bittl, R.; Fromme, P.; Lubitz, W.; Stehlik, D. *J. Phys. Chem. B* **1998**, *102*, 8278.
(11) Zech, S. G.; Hofbauer, W.; Kamlowski, A.; Fromme, P.; Stehlik, D.; Lubitz, W.; Bittl, R. *J. Phys. Chem. B* **2000**, *104*, 9728. See also: van der Est, A.; Prisner, T. F.; Bittl, R.; Fromme, P.; Lubitz, W.; Möbius, K.; Stehlik, D. *J. Phys. Chem. B* **1997**, *101*, 1437.
(12) MacMillan, F.; Hanley, J. van der Weerd, L.; Knüpling, M.; Un, S.; Rutherford, A. W. *Biochemistry* **1997**, *36*, 9297.
(13) Isaacson, R. A.; Lendzian, F.; Abresch, E. C.; Lubitz, W.; Feher, G. *Biophys. J.* **1995**, *69*, *311*.
(14) Review: Lubitz, W.; Feher, G. *Appl. Magn. Reson.* **1999**, *17*, 1.
(15) Review: Levanon, H.; Möbius, K. *Annu. Rev. Biophys. Biomol. Struct.* **1997**, *26*, 495.
(16) Most qualitative discussions of **g**-tensors for organic π-radicals are based on the theory of Stone: Stone, A. J. *Proc. R. Soc. A* **1963**, *271*, 424. Stone, A. J. *Mol. Phys.* **1964**, *6*, 316.
(17) Zandstra, P. J. *J. Chem. Phys.* **1964**, *41*, 3655. This is probably the first report of solvent effects on (isotropic) *g*-values of semiquinones.
(18) See also: Yonezawa, T.; Kawamura, T.; Ushio, M.; Nakao, Y. *Bull. Chem. Soc. Jpn.* **1970**, *43*, 1022.
(19) Engström, M.; Vahtras, O.; Ågren, H. *Chem. Phys.* **1999**, *243*, 263.
(20) Angstl, R. *Chem.* Phys. **1989**, *132*, 435. Plakhutin, B. N.; Zhidomirov, G. M.; Zamaraev, K. I. *J. Struct. Chem.* **1983**, *24*, 3.
(21) Un, S.; Atta, M.; Fontcave, M.; Rutherford, A. W. *J. Am. Chem. Soc.* **1995**, *117*, 10713.
(22) Knüpling, M.; Törring, J. T.; Un, S. *Chem. Phys.* **1996**, *219*, 291.
(23) Törring, J. T.; Un, S.; Knüpling, M.; Plato, M.; Möbius, K. *J. Chem. Phys.* **1997**, *107*, 3905.
(24) Malkina, O. L.; Vaara, J.; Schimmelpfennig, B.; Munzarová, M.; Malkin, V. G.; Kaupp, M. *J. Am. Chem. Soc.* **2000**, *122*, 9206.

influence of hydrogen bonding on the **g**-tensors, as well as the effects of the substituents, is analyzed quantitatively, including conformational effects. We thereby also obtain a detailed assessment of the accuracy of the underlying computational approach. The computational results are then used to point out some pecularities of **g**-tensors measured for semiquinone radical anions substituted into photosystem I.

Theory

Details of our density-functional theory (DFT) method for the calculation of electronic **g**-tensors have been given in ref 24. Here we only summarize the salient features. The **g**-tensor is calculated as correction to the free electron value (given in ppm)[25], i.e.,

$$\mathbf{g} = g_e\mathbf{1} + \Delta\mathbf{g} \tag{1}$$

with $g_e = 2.002\,319$. Up to the level of second-order perturbation theory, the **g**-shift $\Delta\mathbf{g}$ consists of the relevant Breit-Pauli terms[26]

$$\Delta\mathbf{g} = \Delta\mathbf{g}_{SO/OZ} + \Delta\mathbf{g}_{RMC} + \Delta\mathbf{g}_{GC} \tag{2}$$

of which the "paramagnetic" second-order spin−orbit/orbital Zeeman cross term, $\Delta\mathbf{g}_{SO/OZ}$, dominates (except for extremely small Δg-values). Within the present approach[24] (for a clear discussion of the relation between modern ab initio approaches and Harriman's derivations, see ref 27), its Cartesian components u,v are computed as

$$\Delta g_{SO/OZ,uv} = \frac{\alpha^2}{2} g_e \left[\sum_k^{occ(\alpha)} \sum_a^{virt(\alpha)} \frac{\langle \psi_k^\alpha | H_{SO,v} | \psi_a^\alpha \rangle \langle \psi_a^\alpha | l_{O,u} | \psi_k^\alpha \rangle}{\epsilon_k^\alpha - \epsilon_a^\alpha - \Delta E_{k\to a}^{xc}} - \sum_k^{occ(\beta)} \sum_a^{virt(\beta)} \frac{\langle \psi_k^\beta | H_{SO,v} | \psi_a^\beta \rangle \langle \psi_a^\beta | l_{O,u} | \psi_k^\beta \rangle}{\epsilon_k^\beta - \epsilon_a^\beta - \Delta E_{k\to a}^{xc}} \right] \tag{3}$$

$\Delta E_{k\to a}^{xc}$ is the correction term of sum-over-states density functional perturbation theory (SOS-DFPT).[28] By setting $\Delta E_{k\to a}^{xc} = 0$, we arrive at the uncoupled DFT (UDFT) approach. The spin−orbit (SO) operator H_{SO}[29] is computed in the atomic mean-field approximation (AMFI).[30,31] This approach has been shown[24] to give results to within better than a few percent of the exact Breit-Pauli one- and two-electron SO−Hamiltonian, at a small fraction of the computational effort required for the latter (among many other quantities, this holds also for SO corrections to NMR chemical shifts)[32,33]. The AMFI SO operators are therefore applicable to large systems. As a consequence, the SO-operators are not anymore expected to constitute a major source of errors nor a computational bottleneck in our **g**-tensor calculations. We note that, in contrast to the usual treatment of SO operators in currently used standard DFT approaches, our use of both explicit 1- and 2-electron SO mean-field integrals does cover the spin-other-orbit terms resulting from the Breit interaction. In the case of organic radicals, this term may account for as much as 25% of the two-electron SO contributions.[24] The relativistic mass correction term $\Delta\mathbf{g}_{RMC}$ and the one-electron part of the gauge correction term $\Delta\mathbf{g}_{GC}$ are also included in our approach.[24]

3. Computational Details

Figure 1 shows the paraquinones from which the semiquinone radical anions studied here derive, together with a number of biologically relevant systems: Plastoquinone-9 (PQ-9) is the primary electron-transfer acceptor in PS−II, ubiquinone-10 (UQ-10) is the primary acceptor in bRC, and phylloquinone (Vitamin K_1; Vit K_1) performs this function in PS−I. As the isoprenoid side chains in these three systems are not expected to influence the **g**-tensors of the semiquinones appreciably,[6] simplified models may be studied, both experimentally[6−8] and computationally (cf. arrows in Figure 1). In particular, the trimethyl-substituted benzoquinone (TMQ) and dimethylethylbenzoquinone (DMEQ) should serve as reasonable models for PQ-9. The dimethoxy-dimethyl system (UQ-M) models UQ-10, and dimethylnaphthoquinone (DMNQ) approximates Vit K_1. To study substituent effects in more detail, the radical anions of unsubstituted benzoquinone (BQ), of dimethyl-benzoquinone (DMBQ), of tetramethyl-benzoquinone (duroquinone, DQ), and of naphthoquinone (NQ) have also been included in our study. Almost the same series of semiquinone radical anions has recently been studied by W-band EPR spectroscopy,[6] and by Q-band EPR and by ENDOR,[8] in frozen 2-propanol solution. This allows the direct, systematic comparison with experiment. A variety of these species has already been the subject of semiempirical **g**-tensor calculations[22] (previous DFT work on hyperfine coupling constants will be addressed in sections 4 and 5).

All structures have been optimized at the gradient-corrected DFT level (BP86 functional),[34] using the Gaussian98 program.[35] The optimizations employed effective core potentials (ECPs) and DZP valence basis sets for the non-hydrogen atoms,[36] and a DZV hydrogen basis.[37] The use of ECPs has been motivated by parallel investigations of the interactions of semiquinones with metal centers and is expected to affect the optimized structures negligibly. Harmonic vibrational frequency analyses for $DQ^{\bullet-}$ were carried out at the same computational level.

Conformational profiles for the rotation of one methoxy group in $UQ\text{-}M^{\bullet-}$ (section 5) were obtained by varying the relevant dihedral angle θ in steps of typically 10° and reoptimizing all other degrees of freedom without symmetry restrictions. In contrast, the corresponding

(25) i.e., deviations from the free-electron value are provided in units of 10^{-6}.
(26) Harriman, J. E. *Theoretical Foundations of Electron Spin Resonance*; Academic Press: New York, 1978.
(27) Lushington, G. *Ph.D. Thesis*, University of New Brunswick, Canada, 1991.
(28) Malkin, V. G.; Malkina, O. L.; Casida, M. E.; Salahub, D. R. *J. Am. Chem. Soc.* **1994**, *116*, 5898. Malkin, V. G.; Malkina, O. L.; Eriksson, L. A.; Salahub D. R. in *Modern Density Functional Theory: A Tool for Chemistry; Theoretical and Computational Chemistry*; Seminario, J. M., Politzer, P., Eds.; Elsevier, Amsterdam, 1995; Vol. 2.
(29) In eq 3, only a component of the spatial part of H_{SO} is indicated. Prefactors are given in front of the brackets.
(30) Hess, B. A.; Marian, C. M.; Wahlgren, U.; Gropen, O. *Chem. Phys. Lett.* **1996**, *251*, 365.
(31) The AMFI code used is due to: Schimmelpfennig, B. *Atomic Spin−Orbit Mean-Field Integral Program*; Stockholms Universitet, Sweden 1996.
(32) Malkina, O. L.; Schimmelpfennig, B.; Kaupp, M.; Hess, B. A.; Chandra, P.; Wahlgren, U.; Malkin, V. G. *Chem. Phys. Lett.* **1998**, *296*, 93.
(33) Vaara, J.; Malkina, O. L.; Stoll, H.; Malkin, V. G.; Kaupp, M. *J. Chem. Phys.* **2001**, 114, 61.
(34) Becke, A. D. *Phys. Rev. A* **1988**, *38*, 3098. J. P. Perdew *Phys. Rev. B* **1986**, *33*, 8822.
(35) Frisch, M. J.; Trucks, G. W.; Schlegel, H. B.; Scuseria, G. E.; Robb, M. A.; Cheeseman, J. R.; Zakrzewski, V. G.; Montgomery, J. A., Jr.; Stratmann, R. E.; Burant, J. C.; Dapprich, S.; Millam, J. M.; Daniels, A. D.; Kudin, K. N.; Strain, M. C.; Farkas, O.; Tomasi, J.; Barone, V.; Cossi, M.; Cammi, R.; Mennucci, B.; Pomelli, C.; Adamo, C.; Clifford, S.; Ochterski, J.; Petersson, G. A.; Ayala, P. Y.; Cui, Q.; Morokuma, K.; Malick, D. K.; Rabuck, A. D.; Raghavachari, K.; Foresman, J. B.; Cioslowski, J.; Ortiz, J. V.; Stefanov, B. B.; Liu, G.; Liashenko, A.; Piskorz, P.; Komaromi, I.; Gomperts, R.; Martin, R. L.; Fox, D. J.; Keith, T.; Al-Laham, M. A.; Peng, C. Y.; Nanayakkara, A.; Gonzalez, C.; Challacombe, M.; Gill, P. M. W.; Johnson, B. G.; Chen, W.; Wong, M. W.; Andres, J. L.; Head-Gordon, M.; Replogle, E. S.; Pople, J. A. *Gaussian 98*, revision *A.7, A.9*; Gaussian, Inc.: Pittsburgh, PA, 1998.
(36) Bergner, A.; Dolg, M.; Küchle, W.; Stoll, H.; Preuss, H. *Mol. Phys.* **1993**, *80*, 1431. d-functions were taken from: *Gaussian Basis Sets for Molecular Calculations*; Huzinaga, S., Ed.; Elsevier: New York, 1984.
(37) Godbout, N.; Salahub, D. R.; Andzelm, J.; Wimmer, E. *Can. J. Chem.* **1992**, *70*, 560.

calculations for $DQ^{\bullet-}$ rotated all four methyl groups simultaneously in the direction indicated by the lowest-energy methyl-group rotation mode (A_{2u} symmetry), obtained from harmonic vibrational frequency analysis at the D_{2h} symmetrical minimum structure. For each value of the methyl-group dihedral angle ϕ, all other degrees of freedom have been reoptimized within the constraints of D_2 symmetry. Similarly, the profiles of energy, Δg_{xx}, and hydrogen-bond distance as functions of the out-of-plane angle of the hydrogen bond in $BQ^{\bullet-}(H_2O)$ were obtained by varying the dihedral angle γ in steps of 10° and reoptimizing all other degrees of freedom.

The **g**-tensor calculations were carried out with the deMon program,[28,38] and its recently implemented **g**-tensor module.[24] Both UDFT calculations and SOS-DFPT calculations (in the Loc.1 approximation[28]) employed the BP86 functional.[34] Gradient-corrected functionals have been shown previously to be superior to local density functionals in the calculation of **g**-tensors for main group systems.[24,39] In most calculations, we employed a DZVP all-electron basis set,[37] which has been shown to provide accurate **g**-tensor results for other aromatic radicals.[24] Test calculations for benzosemiquinone, with the larger basis sets BII and BIII of Kutzelnigg et al. (also known as IGLO−II and IGLO−III[40]) based on the earlier work of Huzinaga,[41] are provided in section 5. Auxiliary basis sets for the fit of exchange-correlation potential and charge density were of the sizes 5,2 for C, N, and O and 5,1 for H (*n*,*m* denotes *n* s-functions and *m* spd-shells with shared exponents).[38] A compromise strategy discussed earlier[28] was applied to obtain accurate Kohn−Sham MOs with moderate effort, by adding an extra iteration with a larger integration grid and without fit of the exchange-correlation potential after initial SCF convergence has been reached. FINE angular grids with 32 points of radial quadrature were used.[38] The influence of the fit on the results has been tested in some preliminary calculations using our new program system ReSpect,[42] which allows calculations without fitting. The fit reduces Δg_{xx} systematically by ca. 3% but has no significant effect on the other components (similar observations have been made for NMR chemical shifts).[43] As the underlying localization procedures of an IGLO approach[40] to the magnetic gauge problem turned out to produce numerical artifacts for the delocalized open-shell systems studied, we have preferred a common gauge origin at the center of mass throughout the present study. This is justified by the overall low gauge dependence[24,27,39] of the **g**-tensor (compared to, e.g., the NMR chemical shift tensor), and it has been verified by further test calculations with different choices of gauge origin. We generally follow the notation for the semiquinone **g**-tensor components as employed in the literature, i.e., g_{xx} is oriented along the carbonyl C−O bond vector, g_{yy} is in the molecular plane but perpendicular to the C−O vector, and g_{zz} is perpendicular to the semiquinone plane. We note in passing that for the systems studied here, the orientation of Δg_{xx} does generally not deviate noticeably from these idealized orientations.

4. Results of Structure Optimizations

The structures of many substituted semiquinone radical anions, as well as their hydrogen-bonded complexes with one or more 2-propanol or water molecules, have been fully optimized. Tables with full Cartesian coordinates are available as Supporting Information. There have been several previous DFT studies of structures, as well as IR data, hyperfine couplings, and redox properties of various semiquinones.[44−48] In those cases where direct comparison is possible, our structural data agree well with these prior investigations. We will hence restrict the discussion to those main structural features that will be relevant for understanding the **g**-tensor data. This concerns in particular the conformations of substituents and of hydrogen-bonded water and 2-propanol molecules. Some further information on hydrogen bonding is available from ENDOR experiments[7] and from semiempirical (PM3)[44] and DFT[48] calculations on model complexes with water or methanol molecules.

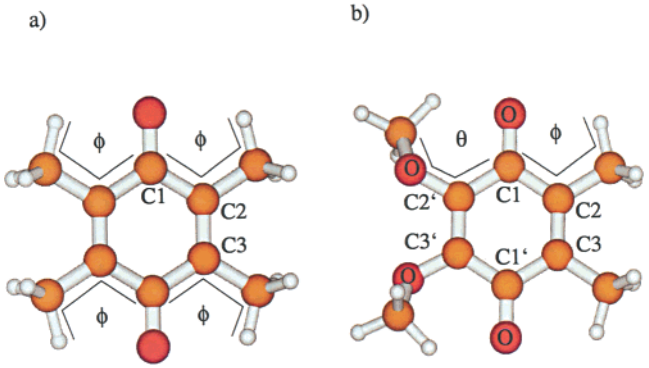

Figure 2. Optimized structures of $DQ^{\bullet-}$ and $UQ\text{-}M^{\bullet-}$, and definition of conformational angles ϕ for methyl and θ for methoxy substituents, respectively. (a) $DQ^{\bullet-}$, (b) $UQ\text{-}M^{\bullet-}$.

Bond lengths within the semiquinone ring systems are known to depend critically on electron correlation. For benzosemiquinone, Hartree−Fock wave functions have been found to give too large weight to the quinoid resonance structures and, e.g., significantly too short C−O bond lengths.[19] The DFT approach used here corrects this deficiency and is expected to provide a reasonable description of structure and bonding. In the case of $BQ^{\bullet-}$, the optimized bond lengths are C1−O = 1.266 Å, C1−C2 = 1.464 Å, and C2−C3 = 1.383 Å, in reasonable agreement with earlier DFT studies.[44a,45a,48] An MP2 optimization with the same ECPs and basis sets gives C1−O = 1.256 Å, C1−C2 = 1.459 Å, and C2−C3 = 1.381 Å, consistent with the DFT data. The DFT-optimized dimensions of the semiquinone ring for the other systems are similar, except for $NQ^{\bullet-}$ and $DMNQ^{\bullet-}$, where the fusion to a second ring increases the C2−C3 distance by ca. 0.05 Å for the bond shared between two rings[45b] and the associated C1−C2 distances by ca. 0.025 Å (cf. atom labeling in Figure 2b). This is accompanied by less significant lengthening and shortening of the remote C1′-C2′ and C2′-C3′ distances, respectively.

Figure 2 shows the optimized structures of unsolvated $DQ^{\bullet-}$ and $UQ\text{-}M^{\bullet-}$, together with the definitions of the out-of-plane dihedral angles ϕ for methyl and θ for methoxy substituents, respectively. The D_{2h} structure with an eclipsed arrangement of the methyl groups in $DQ^{\bullet-}$ is the lowest-energy conformer computed for the free radical anion (Figure 2a). This arrange-

(38) deMon program: Salahub, D. R.; Fournier, R.; Mlynarski, P.; Papai, I.; St-Amant, A.; Ushio, J. in *Density Functional Methods in Chemistry*; Labanowski, J., Andzelm, J., Eds.; Springer, New York, 1991. St-Amant, A.; Salahub, D. R. *Chem. Phys. Lett.* **1990**, *169*, 387.
(39) Schreckenbach, G.; Ziegler, T. *J. Phys. Chem. A* **1997**, *101*, 3388.
(40) Kutzelnigg, W.; Fleischer, U.; Schindler, M. *NMR−Basic Principles and Progress*; Springer, Heidelberg, 1990; Vol. 23, p 165ff.
(41) Huzinaga, S. *Approximate Atomic Functions*; University of Alberta, Canada, 1971.
(42) Program package ReSpect, version 1.0, written by V. G. Malkin, O. L. Malkina, R. Reviakine, B. Schimmelpfennig, A. Arbouznikov, M. Kaupp.
(43) See, e.g., Olsson, L.; Cremer, D. *J. Chem. Phys.* **1996**, *105*, 8995.
(44) (a) O'Malley, P. J. *J. Phys. Chem. A* **1997**, *101*, 6334; (b) O'Malley, P. J. *J. Phys. Chem. A* **1998**, *102*, 248; (c) O'Malley, P. J. *J. Am. Chem. Soc.* **1998**, *120*, 5093.
(45) (a) Eriksson, L. A.; Himo, F.; Siegbahn, P. E. M.; Babcock, G. T. *J. Phys. Chem. A* **1997**, *101*, 9496. (b) Himo, F.; Babcock, G. T.; Eriksson, L. A. *J. Phys. Chem. A* **1999**, *103*, 3745.
(46) Grafton, A. K.; Wheeler, R. A. *J. Phys. Chem. A* **1997**, *101*, 7154. Boesch, S. E.; Wheeler, R. A. *J. Phys. Chem. A* **1997**, *101*, 5799. Wise, K. E.; Grafton, A. K.; Wheeler, R. A. *J. Phys. Chem. A* **1997**, *101*, 1160.
(47) (a) Nonella, M. *J. Phys. Chem. B* **1998**, *102*, 4217. (b) Nonella, M. *Photosynth. Res.* **1998**, *55*, 253.
(48) Zhan, C.-G.; Chipman, D. M. *J. Phys. Chem. A* **1998**, *102*, 1230.

ment appears to maximize hyperconjugative interactions between the aromatic π-system and the σ^*(C−H) orbitals of the methyl substituents and at the same time to minimize the repulsion between the two methyl groups on the same side of the ring. In the absence of hydrogen bonding, the same conformation is preferred for all free radical anions with two methyl groups on the same side (DMBQ$^{\bullet-}$, DMEQ$^{\bullet-}$, UQ-M$^{\bullet-}$, TMQ$^{\bullet-}$, DMNQ$^{\bullet-}$). In contrast, methyl groups without neighboring methyl group, as the one in TMQ, prefer to orient the in-plane hydrogen atom away from the nearest carbonyl group (the β-methyl group in DMEQ$^{\bullet-}$ also points away). The most favorable conformation of free UQ-M$^{\bullet-}$ has the methoxy substituents rotated out of the semiquinone plane on opposite sides, with a dihedral angle θ of ca. 56° (Figure 2b). The significantly out-of-plane orientation agrees very well with previous DFT calculations,[7,45b−47] and differs from the situation for the neutral quinone. The conformer with the two methoxy groups on opposite sides apparently is slightly more favorable than the one with both groups on the same side.[47] However, for both methyl and methoxy substituents, EPR and ENDOR data have suggested almost free rotation even in frozen solution.[8] This is confirmed by our computed conformational energy profiles (cf. section 5). Thus, the computed minima may at best be viewed as snapshots of an intrinsically dynamical situation.

Table 1 provides O···H distances and out-of-plane dihedral angles for the hydrogen bonds in various model complexes. We note in passing that in some cases (e.g., DQ$^{\bullet-}$, DMEQ$^{\bullet-}$, TMQ$^{\bullet-}$, UQ$^{\bullet-}$) the O···H distances differ from earlier estimates based on ENDOR data,[4,8] but they are in good agreement with other computational studies.[44,45a,48] Resolution of the full hyperfine tensors and thus determination of the distances by ENDOR is expected to become more difficult for out-of-plane hydrogen bonding and, in particular, when both in-plane and out-of-plane hydrogen bonds are present simultaneously.[7,8,13]

Figure 3a shows the optimized structure of the complex BQ$^{\bullet-}$(*i*PrOH)$_4$, with two 2-propanol molecules hydrogen-bonded to each carbonyl oxygen atom. The hydrogen bonds are oriented within a few degrees (dihedral angle γ, cf. definition in Figure 3a) from the ring plane [this holds also for the complex BQ$^{\bullet-}$(H$_2$O)$_4$]. We find the same in-plane hydrogen-bonding situation for complexes of BQ$^{\bullet-}$ with a smaller number of hydrogen bonds, as well as for the unsubstituted sides in DMBQ$^{\bullet-}$ and NQ$^{\bullet-}$ (Table 1) Similar conclusions were already reached on the basis of ENDOR data,[8] and of DFT,[48] and PM3[44a] calculations. In contrast, the presence of substituents on the semiquinone ring, near the carbonyl group, is expected[8,44b,c] to force a partial out-of-plane orientation of the hydrogen bonds. This is shown for the example DQ$^{\bullet-}$(*i*PrOH)$_4$ in Figure 3b. All four hydrogen bonds are oriented out of the semiquinone plane ($\gamma = -30°$ to $-46°$), and the in-plane hydrogen atoms of the methyl substituents prefer to point away from the carbonyl groups. In our optimizations we find that the preferred γ is strongly coupled to the orientation (ϕ) of the substituents. Different starting structures frequently lead to different conformers with very similar energies. For example, in the case of DQ$^{\bullet-}$(*i*PrOH)$_4$ a structure with two in-plane hydrogen bonds ($\gamma \approx -2°$; the in-plane hydrogen atoms of the neighboring methyl groups point toward the carbonyl group) and two out-of-plane hydrogen bonds ($\gamma \approx -43°$) is calculated to be only 2.2 kJ mol^{-1} higher in energy (Figure 3c). We therefore expect a dynamical situation, possibly even at low temperatures. This holds for all methyl-substituted systems. The optimized structures in these cases should be viewed with some caution, keeping in mind both the limited numerical accuracy of the structure

Table 1. Computed Structural Features of Hydrogen Bonds to Semiquinone Radical Anions[a]

model, position	d(H···O) in Å	absolute dihedral angle γ with ring plane in deg[b]
BQ$^{\bullet-}$		
+(H$_2$O)$_2$ (same CO)	1.76	4
+(H$_2$O)$_4$	1.79	3
+(*i*PrOH)$_2$ (same CO)	1.70	3−4
+(*i*PrOH)$_4$	1.74	3
exp.[a]	1.78	in-plane
DMBQ$^{\bullet-}$		
+(H$_2$O)$_4$ (pos. 1,2)[c]	1.78	11, 15
(pos. 3,4)[d]	1.78	3−4
+(*i*PrOH)$_4$ (pos. 1,2)[c]	1.75	32,37
(pos. 3,4)[d]	1.71	0−2
exp.[a]	1.79	in-plane
TMQ$^{\bullet-}$		
+(H$_2$O)$_4$ (pos. 1)[d]	1.79	3
(pos. 2,3)[c]	1.77, 1.79	12, 47
(pos. 4)[e]	1.80	47
+(*i*PrOH)$_4$ (pos. 1)[d]	1.71	0
(pos. 2,3)[c]	1.75	18, 40
(pos. 4)[e]	1.76	43
exp.[a]	1.87, 1.94	in-plane, out-of-plane
DMEQ$^{\bullet-}$		
+(H$_2$O)$_4$ (pos. 1)[d]	1.78	5
(pos. 2,3)[c]	1.78, 1.80	30, 50
(pos. 4)[e]	1.80	52
+(*i*PrOH)$_4$ (pos. 1)[d]	1.71	1
(pos. 2,3)[c]	1.75	17, 40
(pos. 4)[e]	1.76	45
exp.[a]	1.87, 1.95	in-plane, out-of-plane
DQ$^{\bullet-}$		
+(H$_2$O)$_2$ (same CO)	1.77	17−18
+(H$_2$O)$_4$	1.80	53
+(*i*PrOH)$_2$ (same CO)	1.71	44
+(*i*PrOH)$_4$	1.72, 1.75	30, 46
exp.[a]	1.87	out-of-plane (ca. 30−40)
NQ$^{\bullet-}$		
+(H$_2$O)$_4$ (pos. 1,2)[f]	1.79	10
(pos. 3,4)[d]	1.80	5−6
+(*i*PrOH)$_4$ (pos. 1,2)[f]	1.76−1.77	24
(pos. 3,4)[d]	1.76	11−12
DMNQ$^{\bullet-}$		
+(H$_2$O)$_4$ (pos. 1,2)[f]	1.79	17
(pos. 3,4)[c]	1.80	40−41
+(*i*PrOH)$_4$ (pos. 1,2)[f]	1.75	21
(pos. 3,4)[c]	1.76	36
UQ-M$^{\bullet-}$		
+(H$_2$O)$_4$ (pos. 1,2)[c]	1.78	14, 34
(pos. 3,4)[g]	1.89, 1.81	19, 21
+(H$_2$O)$_6$ (pos. 1,2)[c]	1.79, 1.80	36, 4
(pos. 3,4)[g]	1.83	21−24
+(*i*PrOH)$_4$ (pos. 1,2)[c]	1.74, 1.71	29, 36
(pos. 3,4)[g]	1.79, 1.76	7, 38
+(*i*PrOH)$_6$ (pos. 1,2)[c]	1.75, 1.74	17, 22
(pos. 3,4)[g]	1.78, 1.75	46, 61
exp. (UQ-9$^{\bullet-}$)[a]	1.89, 1.94	out-of-plane

[a] Optimizations with BP86 functional, ECPs and DZP valence basis sets. Experimental values estimated from ENDOR data in frozen 2-propanol, cf. ref 7. [b] cf., Figures 3 and 4 for the definition of γ. As defined, the dihedral angles have a negative sign in most cases. [c] Positions with two methyl groups on the same side. [d] Positions without methyl substituents on this side. [e] Position with one methyl or ethyl group on this side. [f] Positions with fused benzene ring on the side. [g] Positions with two methoxy groups on the same side.

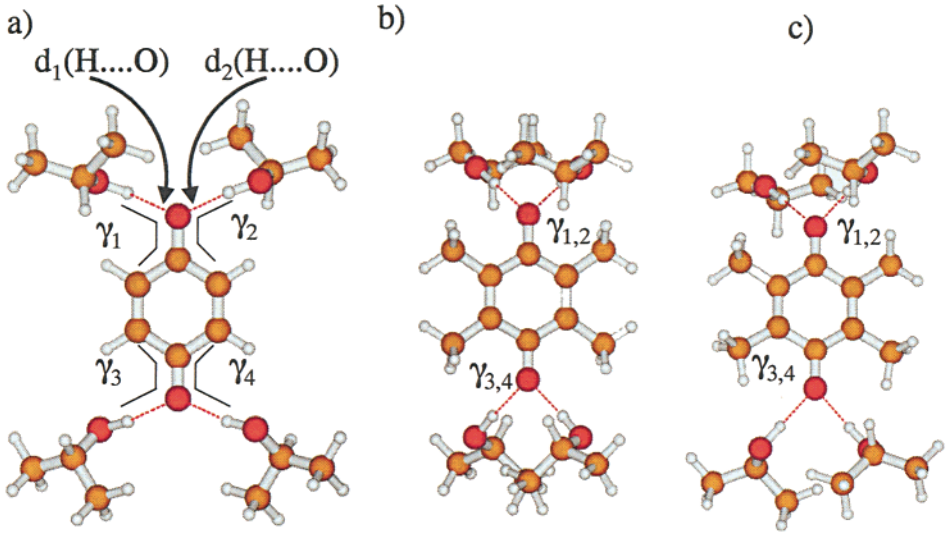

Figure 3. Optimized structures of semiquinone radical anions with four 2-propanol solvent molecules, with definition of out-of-plane dihedral angles γ for hydrogen bonding. (a) $BQ^{\bullet-}(i\text{PrOH})_4$, (b) $DQ^{\bullet-}(i\text{PrOH})_4$, conformation 1, see text. (c) $DQ^{\bullet-}(i\text{PrOH})_4$, conformation 2, see text.

optimizations and the dynamical effects in the real system (e.g., forming and breaking of hydrogen bonds).[48] These factors provide probably some of the main limitations to the accuracy achievable in the **g**-tensor calculations (see section 5).

Table 1 shows that hydrogen bonds oriented partially out-of-plane are also found on the dimethyl-substituted sides of other semiquinones. In those cases, where the dihedral angles for the two hydrogen bonds are appreciably different, the differences correlate with inequivalent conformations of the two methyl substituents. In general, we expect little energy cost for a cooperative change of the conformations. In some cases, notable differences in γ may be seen between water and 2-propanol as donor. On average, the bulkier 2-propanol donors force more strongly out-of-plane arrangements, as one might expect.

In-plane hydrogen bonds are expected to be stronger. This is confirmed by the energy profile of $BQ^{\bullet-}(H_2O)$ as a function of γ (Figure 4a). Indeed, for this example, the hydrogen bond distances increase significantly up to $\gamma \approx 60°$, before leveling off at still larger out-of-plane angles (Figure 4b). As a consequence, distances connected to hydrogen bonds with larger γ values in Table 1 tend to be slightly larger than those with smaller γ. However, the differences are relatively small, and all systems feature two strong hydrogen bonds to each carbonyl group. This result is consistent with earlier semiempirical (PM3) structure optimizations and DFT calculations of hyperfine tensors.[44] EPR or ENDOR studies presently cannot clearly determine the number of hydrogen bonds and, on the other hand, provide a time-averaged picture of the hydrogen-bond exchange processes. For most of the semiquinones in this study (however, cf. UQ-$M^{\bullet-}$ below) we regard complexes with two hydrogen bonds to each carbonyl group as reasonable models of the first solvation shell in isotropic protic solution.

The two hydrogen bonds on the dimethoxy-substituted side in both UQ-$M^{\bullet-}(L)_4$ systems (positions 3 and 4) are oriented on the same side of the ring as the substituents. Steric crowding may be responsible for the particularly large γ of the hydrogen bonds in UQ-$M^{\bullet-}(i\text{PrOH})_6$ on the methoxy-substituted side (Table 1). Interestingly, the methoxy substituents in the solvated UQ-$M^{\bullet-}$ models are oriented much more strongly out-of-plane

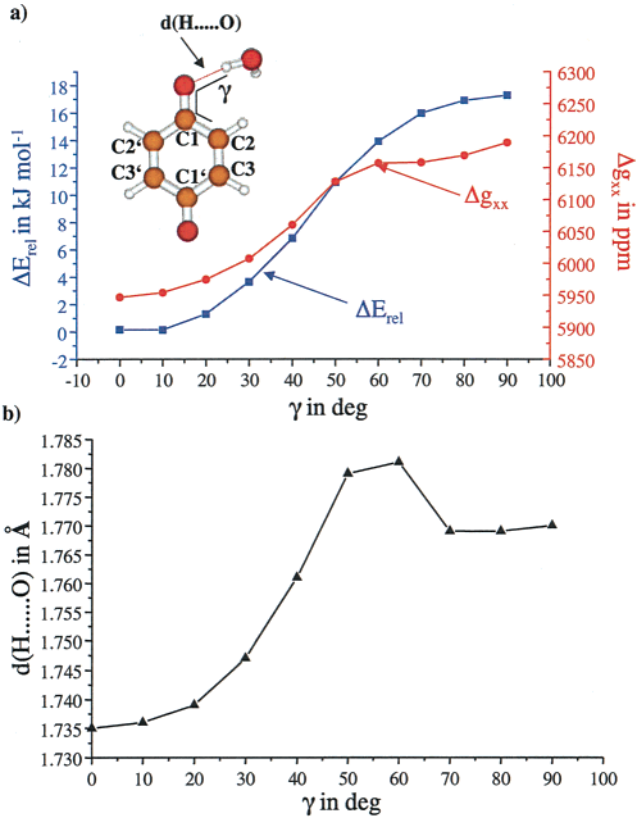

Figure 4. (a) Dependence of relative energy and Δg_{xx} (UDFT-BP86 results) for $BQ^{\bullet-}(H_2O)$ on hydrogen-bonding out-of-plane angle γ. For each value of γ, all other degrees of freedom have been reoptimized. Insert: definition of γ and atom labels. (b) Dependence of hydrogen bond distance on γ.

[$\theta \approx 103°$ for UQ-$M^{\bullet-}(H_2O)_4$; cf. $\theta \approx 110°$ for UQ-$M^{\bullet-}(i\text{PrOH})_4$, $\theta \approx 100°$ for UQ-$M^{\bullet-}(H_2O)_6$, and $\theta \approx 95°$ for UQ-$M^{\bullet-}(i\text{PrOH})_6$] than in the absence of hydrogen bonds ($\theta \approx 56°$, cf. above). This has significant consequences for the **g**-tensor results (cf. section 5).

The computed lengths of the hydrogen bonds to the carbonyl oxygen atoms vary typically in a relatively narrow range, between 1.77 and 1.81 Å for H_2O as hydrogen-bond donor. The complexes with *i*PrOH exhibit consistently somewhat shorter

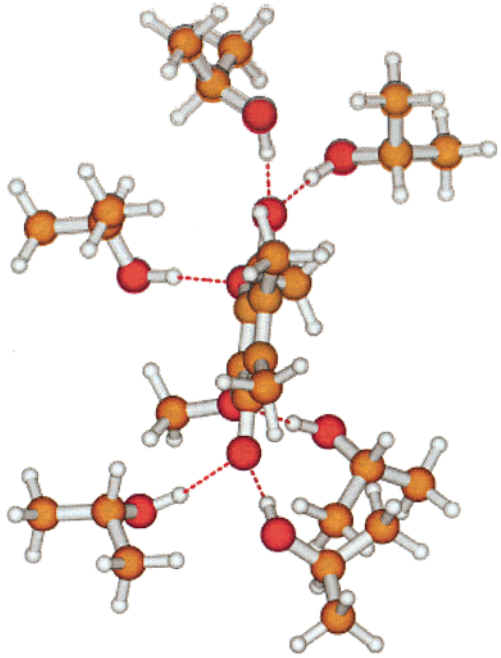

Figure 5. Optimized structure of UQ-M$^{\bullet-}$(iPrOH)$_6$ with extra hydrogen bonds to the methoxy substituents.

bond lengths (typically by ca. 0.04−0.06 Å). This agrees with the expectation that, in the absence of overwhelming steric effects, 2-propanol is intrinsically a somewhat stronger hydrogen-bond donor than water.[49]

The ubisemiquinone systems (UQ-M$^{\bullet-}$ in our calculations) are exceptional in having two methoxy groups, which may act as additional acceptors for hydrogen bonding. Figure 5 shows the optimized structure of UQ-M$^{\bullet-}$(iPrOH)$_6$, in which two hydrogen bonds to each carbonyl group are augmented by one hydrogen bond to each methoxy group. These additional hydrogen bonds are oriented essentially perpendicular to the semiquinone ring. Additional hydrogen bridges between the donors have been found neither in this system nor in the related model UQ-M$^{\bullet-}$(H$_2$O)$_6$. While the hydrogen bonds to the formally sp^3 hybridized methoxy oxygen atoms are on average ca. 0.05 Å longer than those to the carbonyl groups, it is clear that they constitute additional, strong primary hydrogen bonds. We have also tried to attach one more water molecule to each of the two methoxy groups in UQ-M$^{\bullet-}$(H$_2$O)$_6$. However, during optimization, these extra water molecules moved in the direction of the nearest carbonyl groups and formed a hydrogen-bonding network between the first solvation shells at carbonyl and methoxy oxygen atoms (cf. coordinates provided as Supporting Information). We conclude that the solvation of ubisemiquinone systems in protic solvents differs from that of the other semiquinones studied, by including six solvent molecules in the first solvation shell.

5. g-Tensor Results

Table 2 compares the **g**-shift components for BQ$^{\bullet-}$ obtained with different basis sets. As found previously for phenoxyl radicals,[24] the modest DZVP basis set compares well with the larger basis sets BII and BIII. The Δg_{xx} component obtained with DZVP basis is ca. 1% and ca. 2% below the BII and BIII results, respectively. In contrast, the DZVP results for Δg_{yy} are higher than the BII and BIII results by similar amounts. The Δg_{zz} components are dominated by diamagnetic contributions and are too small to be discussed meaningfully. The DZVP basis appears to provide a reasonable compromise between accuracy and computational effort for the larger systems to be studied, and it is used throughout the remainder of this work.

Table 2. Basis Set Effects on Computed **g**-Shift Components (in ppm) for BQ$^{\bullet-}$ [a]

basis	Δg_{iso}	Δg_{xx}	Δg_{yy}	Δg_{zz}
DZVP	3104	6276	3057	−21
	(2941)	(5835)	(3006)	(−20)
BII	3108	6312	3025	−13
	(2938)	(5858)	(2968)	(−13)
BIII	3109	6395	2923	10
	(2947)	(5961)	(2872)	(−8)

[a] DFT results with BP86 functional. UDFT results with SOS-DFPT data in parentheses.

Compared to the experimental **g**-shift tensor of BQ$^{\bullet-}$ in frozen 2-propanol, the UDFT results for the unsolvated radical anion overestimate the most critical and characteristic Δg_{xx} component by ca. 50%, whereas the less sensitive Δg_{yy} is only overestimated by ca. 3%. It is expected[2,3,6,9,13,16,17,22] that hydrogen bonding to the carbonyl oxygen atoms reduces Δg_{xx} significantly (see Introduction). Already one hydrogen bond to one carbonyl group has a significant effect. The profiles of energy and Δg_{xx} (Figure 4a), and of hydrogen-bond distance (Figure 4b) for BQ$^{\bullet-}$(H$_2$O) indicate that both the stability of the hydrogen bond and its influence on Δg_{xx} diminish with increasing out-of-plane angle γ of the hydrogen bond, i.e., relative energy and Δg_{xx} both increase. The slight flattening of the Δg_{xx} curve above $\gamma \approx 60°$ (Figure 4a) may reflect the fact (Figure 4b) that the H···O distance levels off again at larger out-of-plane dihedral angles. Nevertheless, relative to the free radical anion, even a hydrogen bond perpendicular to the semiquinone plane does still reduce Δg_{xx} and thus the **g**-tensor anisotropy significantly. Similar effects of hydrogen bonding on Δg_{xx} are known, e.g., for tyrosyl radicals[21,50] or for nitroxide spin labels.[51] A recent MCSCF calculation on the model complex C$_6$H$_5$O·(H$_2$O) has indicated that even a linear O···H−O arrangement reduces Δg_{xx}, but a bent in-plane structure does this even more effectively.[52] Qualitative models,[3,13,21,22,52] usually based on Stone's theory,[16] explain the reduction of Δg_{xx} by hydrogen bonding via (a) an increased HOMO−SOMO energy difference, and (b) a slight redistribution of spin density away from the carbonyl oxygen atom (see also Discussion in section 6).

Table 3 compares different molecular models for hydrogen bonds to BQ$^{\bullet-}$. As expected (cf. structures in section 4), iPrOH is a more effective hydrogen bond donor and leads to a somewhat larger reduction in Δg_{xx} than a water molecule. Interestingly, with one or two hydrogen bonds, Δg_{yy} is very

(49) The good hydrogen-bonding donor abilities are related to the large gas-phase acidity of iPrOH, due to the stabilization of the conjugated base by negative hyperconjugation (see, e.g., Tuñón, I.; Silla, E.; Pascual-Ahuir, J.-L. *J. Am. Chem. Soc.* **1993**, *115*, 2226, and many references therein).

(50) See, e.g., van Dam, P. J.; Willems, J.-P.; Schmidt, P. P.; Pötsch, S.; Barra, A.-L.; Hagen, W. R.; Hoffman, B. M.; Andersson, K. K.; Gräslund, A. *J. Am. Chem. Soc.* **1998**, *120*, 5080. Schmidt, P. P.; Andersson, K. K.; Barra, A.-L.; Thelander, L.; Gräslund, A. *J. Biol. Chem.* **1996**, *271*, 23615.

(51) See, e.g., Lebedev, Ya. S. in *Modern Pulsed and Continuous Wave Electron Spin Resonance*; Kevan, L.; Bowman, M. K., Eds.; Wiley: New York, 1990.

(52) Engström, M.; Himo, F.; Gräslund, A.; Minaev, B.; Vahtras, O.; Ågren, H. *J. Phys. Chem. A* **2000**, *104*, 5149.

Table 3. Influence of Hydrogen Bonding on **g**-Shift Components (in ppm) of $BQ^{\bullet-}$ [a]

model	Δg_{iso}	Δg_{xx}	Δg_{yy}	Δg_{zz}
no H-bond	3104	6276	3057	−21
	(2941)	(5835)	(3006)	(−20)
+ H_2O	2997	5951	3044	−4
	(2846)	(5534)	(3007)	(−3)
+ *i*PrOH	2998	5886	3088	20
	(2847)	(5477)	(3047)	(18)
+$(H_2O)_2$ (same CO)	2935	5762	3041	2
	(2784)	(5340)	(3007)	(6)
+(*i*PrOH)$_2$ (same CO)	2955	5701	3127	37
	(2811)	(5295)	(3101)	(37)
+$(H_2O)_3$ (same CO)	3049	5948	3098	101
	(2886)	(5510)	(3053)	(95)
+$(H_2O)_2$ (1 on each CO)	2812	5448	2991	−3
	(2693)	(5118)	(2963)	(−3)
+$(H_2O)_4$ (2 on each CO)	2570	4776	2931	2
	(2482)	(4547)	(2902)	(−3)
+(*i*PrOH)$_4$ (2 on each CO)	2446	4506	2882	−49
	(2398)	(4393)	(2853)	(−52)
+$(H_2O)_6$ (3 on each CO)	2684	4878	2971	204
	(2614)	(4698)	(2942)	(201)
exp.[b]	2350	4130	2940	−30

[a] UDFT results with SOS-DFPT results in parentheses. [b] In frozen *i*PrOH (ref 6).

slightly reduced for H_2O but slightly increased for the bulkier *i*PrOH. These differences disappear, however, for the more realistic models with two hydrogen bonds to each of the carbonyl groups. Now both components are reduced compared to the free radical anion.

Returning to the effect of hydrogen bonding on Δg_{xx} (Table 3), it is notable that the reduction due to the first hydrogen bond is ca. 5% (ca. 6%) for H_2O (*i*PrOH). A second hydrogen bond to the same carbonyl group is less effective and provides another 3% in both cases, whereas the coordination of a water molecule to the other carbonyl group produces a much larger effect (8%). For the $BQ^{\bullet-}(H_2O)_4$ and $BQ^{\bullet-}$(*i*PrOH)$_4$ models, the overall reduction of Δg_{xx} due to solvation is ca. 24% and ca. 28%, respectively. This is more than twice the effect of two hydrogen bonds to the same carbonyl group but slightly less than twice the effect of two hydrogen bonds to opposite sides.

The resulting values for the most realistic models with four hydrogen bonds are already relatively close to the experimental value in frozen isopronanol [ca. 16% too large for $BQ^{\bullet-}(H_2O)_4$ and only ca. 9% too large for $BQ^{\bullet-}$(*i*PrOH)$_4$]. The final Δg_{yy} values for the $BQ^{\bullet-}$(solvent)$_4$ systems are only slightly below experiment. We note that the SOS-DFPT correction reduces Δg_{xx} further by ca. 3−5% and thus brings this component into even closer agreement with experimental values (this is due to the reduction of the energy denominators in eq 3). However, the overall linear correlation between computed and experimental values is not improved (see below), and we will in the following concentrate on the UDFT results.

In view of these results for the $BQ^{\bullet-}$ system, we expect significantly too large Δg_{xx} for unsolvated semiquinone radical anions, much closer agreement with the experimental data in frozen 2-propanol for systems with four hydrogen bonds, and slightly lower (and thus better) results for the more realistic *i*PrOH compared to H_2O donors. Moreover, Δg_{yy} is expected to be influenced less by hydrogen bonding. These expectations are indeed borne out by the results for the entire series of unsolvated and tetrasolvated systems in Table 4. However, the systematic comparison reveals significantly more information, and interesting differences between various substituted semiquinone radical anions are found.

Figure 6 compares computed Δg_{xx} values for both unsolvated semiquinones and their tetraaqua-complexes with experimental data in frozen 2-propanol. As expected, Δg_{xx} for the free radical anions is generally significantly too large. The deviations from a linear correlation with experimental values are also particularly pronounced for the unsolvated models (cf. Table 5). The most notable outlier is the UQ-$M^{\bullet-}$ model (compared to the experimental results for UQ-$10^{\bullet-}$), placed significantly below the regression line, i.e., the computed result is in apparently "too good" agreement with experimental values. This deviation may be rationalized by a structural effect. As has been discussed in section 4, the methoxy groups may rotate almost freely around the $C-OCH_3$ bond. Moreover, in the unsolvated model, the optimum out-of-plane angle θ is only ca. 56°, whereas the methoxy groups are forced further out-of-plane by hydrogen bonding (in both tetra- and hexasolvated models, the preferred θ is ca. 95−110°). As shown in Figure 7, the dihedral angle θ has a remarkably large effect on Δg_{xx} in UQ-$M^{\bullet-}$ (a smaller one on Δg_{yy}; cf. Supporting Information). This is due to antibonding interactions between oxygen lone pairs on the methoxy groups and the delocalized SOMO. In going from the equilibrium value of θ for the free radical anion to the larger values preferred in the presence of hydrogen bonding, Δg_{xx} increases by more than 300 ppm. The actual effect in solution is expected to be even larger. The potential energy scan of Figure 7 changes only θ_1 for one of the two methoxy groups (in these optimizations, the second group is free to adapt to the new conformation but remains at lower values of θ_2 for a large range of θ_1-values of the first group). If we force both dihedral angles to be $\theta = 110°$, similar to the solvated models, the computed UDFT result for Δg_{xx} is 5676 ppm rather than 5034 ppm. Using this higher value instead, the linear correlation improves significantly (Table 5). The slope increases from 1.097 to 1.483. We believe that the closeness of the former value to 1.0 is completely fortuitous, and that the latter value represents better the significant overestimate of $\Delta g_{xx,SOC/OZ}$ by the unsolvated models.

The previous example shows that dynamical changes of the substituent conformations may have a significant effect on the **g**-tensors. This holds also for methyl group rotations, as shown in Figure 8 for unsolvated $DQ^{\bullet-}$. In this case, however, the equilibrium conformation of the unsolvated radical exhibits a relatively large Δg_{xx} value, whereas other conformations tend to reduce Δg_{xx}. Here we have moved all four methyl groups simultaneously along the D_2-symmetrical pathway indicated by the lowest-energy methyl-group rotation mode (A_{2u}), as obtained from the harmonic vibrational analysis at the D_{2h} symmetrical equilibrium structure. ENDOR data indicate that the rotation of the methyl substituents is also essentially unhindered. This is confirmed by the computed low activation barrier shown in Figure 8. The figure shows also that this motion is expected to lead to a slight *reduction* of Δg_{xx} compared to the value at equilibrium dihedral angle ϕ. This should be compared to the more pronounced *increase* found for the rotation of the methoxy groups in UQ-$M^{\bullet-}$. The opposite direction of the effect may be rationalized by the fact that delocalization between the π-system and the methyl substituents is due to hyperconjugation, an *attractive* two-electron interaction. This contrasts to the *repulsive*

Table 4. Computed **g**-Shift Components for Semiquinone Radical Anions (ppm) with and without Hydrogen Bonding[a]

	UDFT				SOS-DFPT			
	Δg_{iso}	Δg_{xx}	Δg_{yy}	Δg_{zz}	Δg_{iso}	Δg_{xx}	Δg_{yy}	Δg_{zz}
$BQ^{\bullet-}$								
free	3104	6276	3057	−21	2941	5835	3006	−20
$+(H_2O)_4$	2570	4776	2931	2	2482	4547	2902	−68
$+(i\text{PrOH})_4$	2446	4506	2882	−49	2398	4393	2853	−52
exp. (in *i*PrOH)[b]	2350	4130	2940	−30	2350	4130	2940	−30
$DMBQ^{\bullet-}$								
free	2994	5930	3056	−3	2851	5537	3018	−3
$+(H_2O)_4$	2439	4555	2797	−33	2363	4347	2775	−32
$+(i\text{PrOH})_4$	2264	4218	2712	−136	2219	4097	2690	−131
exp. (in *i*PrOH)[b]	2240	3870	2900	−60	2240	3870	2900	−60
$TMQ^{\bullet-}$								
free	2840	5530	3001	−12	2707	5157	2975	−11
$+(H_2O)_4$	2337	4348	2768	−106	2254	4120	2742	−100
$+(i\text{PrOH})_4$	2216	4154	2637	−143	2167	4006	2626	−132
$DMEQ^{\bullet-}$								
free	2865	5592	3006	−3	2731	5215	2982	−4
$+(H_2O)_4$	2322	4320	2762	−116	2237	4088	2736	−112
$+(i\text{PrOH})_4$	2186	4089	2616	−146	2133	3938	2597	−136
exp. ($DMEQ^{\bullet-}$ in *i*PrOH)[b]	2160	3820	2800	−130	2160	3840	2800	−130
exp. ($PQ\text{-}9^{\bullet-}$ in *i*PrOH)[b,c]	2300	4000	2900	0	2300	4000	2900	0
exp. ($PQ\text{-}1^{\bullet-}$ in *i*PrOH)[b,c]	2170	3780	2800	−60	2170	3780	2800	−60
$DQ^{\bullet-}$								
free	2785	5347	3021	−14	2658	4998	2992	−14
$+(H_2O)_4$	2270	4200	2807	−195	2186	3959	2780	−180
$+(i\text{PrOH})_4$	2071	3932	2549	−267	2012	3751	2534	−250
exp. (in *i*PrOH)[b]	2160	3790	2800	−100	2160	3790	2800	−100
exp. (in MTHF)[d]	2380	4380	2910	−140	2380	4380	2910	−140
exp. (in Zn-bRC)[c,e]	2200	3800	2800	0	2200	3800	2800	0
exp. (in PS−I)[c,f]	3000	5000	4000	0	3000	5000	4000	0
$NQ^{\bullet-}$								
free	2795	5464	2896	−25	2677	5133	2873	25
$+(H_2O)_4$	2233	4064	2632	3	2173	3896	2619	5
$+(i\text{PrOH})_4$	2167	3856	2617	29	2135	3779	2599	26
exp. (in *i*PrOH)[b]	2060	3500	2730	−40	2060	3500	2730	−40
exp. (in Zn-bRC)[c,e]	2100	3500	2800	0	2100	3500	2800	0
exp. (in PS−I)[c,f]	2700	4400	3700	0	2700	4400	3700	0
$DMNQ^{\bullet-}$								
free	2445	4587	2750	−2	2345	4312	2729	−5
$+(H_2O)_4$	1992	3630	2487	−140	1934	3450	2480	−128
$+(i\text{PrOH})_4$	2007	3633	2444	−57	1968	3512	2434	−43
exp. ($DMNQ^{\bullet-}$ in *i*PrOH)[b]	1970	3360	2650	−100	1970	3360	2650	−100
exp. ($Vit\text{-}K_1^{\bullet-}$ in *i*PrOH)[b]	1930	3320	2620	−150	1930	3320	2620	−150
exp. ($A_1^{\bullet-}$ in PS−I)[g]	2270	3930	2710	−49	2270	3800	2600	400
exp. ($A_1^{\bullet-}$ in PS−I, transient)[h]	2270	3900	2750	−140	2270	3900	2800	−100
$UQ\text{-}M^{\bullet-}$								
free	2738	5034	3255	−75	2631	4746	3227	2
(with θ fixed to 110°)	2982	5676	3276	−6	2837	5277	3244	−11
$+(H_2O)_4$	2467	4436	2991	−27	2380	4202	2965	−26
$+(H_2O)_6$	2540	4622	2990	8	2451	4382	2962	10
$+(i\text{PrOH})_4$	2416	4320	2961	−34	2375	4214	2950	−37
$+(i\text{PrOH})_6$	2539	4621	2953	44	2493	4499	2953	44
exp. ($UQ\text{-}10^{\bullet-}$ in *i*PrOH)[b]	2380	4140	3100	−100	2380	4140	3100	−100
exp. ($UQ\text{-}3^{\bullet-}$ in *i*PrOH)[i]	2210	3900	2940	−220	2210	3900	2940	−220
exp. ($UQ\text{-}3^{\bullet-}$ in MTHF)[i]	2480	4680	3050	−300	2480	4680	3050	−300
exp. ($Q_A^{\bullet-}$ in Zn-bRCs[b,c])	2400	4300	3100	−100	2400	4300	3100	−100
exp. ($Q_A^{\bullet-}$ in Zn-bRCs[c,j])	2320	4170	3000	−220	2320	4170	3000	−220
exp. ($Q_B^{\bullet-}$ in Zn-bRCs[c,j])	2230	3940	2950	−220	2230	3940	2950	−220

[a] BP86 results with common gauge at center of mass. [b] W-band EPR in frozen 2-propanol, cf. ref 6. [c] Only accurate to ca. ±100 ppm. [d] In aprotic solvent (frozen 1-methyltetrahydrofuran, see ref 6). [e] K-band spectra of radicals reconstituted into Zn-bRCs.[9] [f] K-band spectra of radicals reconstituted into PS−I.[9] [g] Photoaccumulated $A_1^{\bullet-}$ at 283 GHz.[12] [h] Transient spin-polarized W-band EPR on $P_{700}^{\bullet+}A_1^{\bullet-}$ in a PS−I single crystal.[11] [i] Q-band EPR in 2-propanol-d_8 or DME/MTHF mixtures, respectively.[7] [j] Q-band EPR in zinc-substituted reaction centers of *Rb. sphaeroides* R-26, with fully deuterated $UQ\text{-}10^{\bullet-}$.[13]

interactions that dominate for methoxy substituents. Conformational effects on Δg_{yy} are also notable but less pronounced. Methyl-group rotation in $DQ^{\bullet-}$ decreases Δg_{yy} from 3021 ppm at $\phi = 0°$ to 2880 ppm at $\phi = 60°$. Rotation of one methoxy group in $UQ\text{-}M^{\bullet-}$ leads to a relatively small variation of Δg_{yy} between 3255 and 3301 ppm. In both cases, the profiles for Δg_{yy} (cf. Supporting Information) follow largely those for Δg_{xx} in Figures 7 and 8, respectively. It has to be kept in mind that, in the real situation in solution, these effects of substituent conformation are coupled to the orientation of the hydrogen-bonding interactions (cf. section 4). This provides further contributions to the **g**-shift values, in particular for Δg_{xx}, and renders quantitative predictions more difficult. The large effect of the conformation of methoxy groups on both g_{xx} and g_{yy} in ubisemiquinones may be particularly important for the interpretation of the **g**-tensors in many biological systems, including

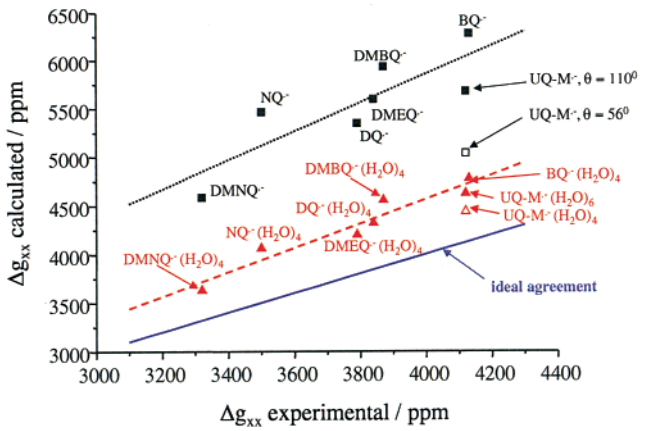

Figure 6. Plot of computed vs experimental Δg_{xx} (UDFT-BP86 results). Unsolvated models (dotted regression line; filled squares) and model water complexes (dashed regression line; filled triangles) are compared. See text for further explanations. The solid line represents ideal correspondence between calculation and experiment.

bacterial reaction centers. Notably, the preferred conformations of the methoxy substituents in ubisemiquinones are expected to influence also the Q/Q$^{\bullet-}$ redox potential.[47b]

Turning to the models with four hydrogen bonds from water molecules, we see in Figure 6 that in all cases Δg_{xx} is reduced significantly compared to the free radical anions. Moreover, the linear correlation with experimental values is improved considerably (Table 5). The most pronounced outlier to low values ("too good" agreement with experimental values) is again provided by the UQ-M$^{\bullet-}$ model. This is again related to the presence of the methoxy substituents. As shown in Table 4, two extra hydrogen bonds from the two methoxy groups to water molecules 5 and 6 increase Δg_{xx} by almost 200 ppm. Taking this more realistic UQ-M$^{\bullet-}$(H$_2$O)$_6$ model as a basis for the linear regression (cf. filled triangles in Figure 6), we arrive at an improved correlation and a larger slope (Table 5). Figure 9 compares the performance of the Q$^{\bullet-}$(H$_2$O)$_4$ models with more elaborate models including four 2-propanol molecules [Q$^{\bullet-}$(*i*PrOH)$_4$]. Due to the stronger hydrogen bonds (cf. section 4), Δg_{xx} is reduced even further. The Q$^{\bullet-}$(*i*PrOH)$_4$ model systems yield an improved linear correlation and a smaller slope (Table 5). Inclusion of two more hydrogen bonds to the methoxy substituents in UQ-M$^{\bullet-}$(*i*PrOH)$_6$ increases Δg_{xx} by 300 ppm (Table 4) and improves the correlation to $R = 0.969$ (with a slope of 1.128). We note in passing that the computed reduction of Δg_{xx} by hydrogen bonding is more pronounced than in earlier semiempirical calculations.[22]

It is apparent that the calculations describe the influence of substituents on the *g*-shift components well, provided that adequate account is taken of hydrogen bonding and of conformational effects. In agreement with experimental values, the lowest Δg_{xx} components are found for DMNQ$^{\bullet-}$, due to the delocalization of spin density into the condensed benzene ring[3,13,22] *and* due to the hyperconjugative effects of the two methyl groups. Consequently, unsubstituted NQ$^{\bullet-}$ exhibits already somewhat larger values. Compared to the parent BQ$^{\bullet-}$, methyl substitution also reduces the Δg_{xx} and Δg_{yy} components in DMBQ$^{\bullet-}$, TMQ$^{\bullet-}$, DMEQ$^{\bullet-}$, and DQ$^{\bullet-}$, and thus the unsubstituted BQ$^{\bullet-}$ system is at the upper end of the scale. We have previously noted the unexpectedly large reduction of Δg_{xx} in phenoxyl radicals by alkyl substitution.[24] Finally, the ubisemiquinone model systems are special due to the presence of methoxy substituents. The latter influence the **g**-shift components both by direct electronic effects (repulsive interactions between oxygen lone pairs and the semiquinone π-type SOMO) and by their ability to accept additional hydrogen bonds. The latter point leads to Δg_{xx} values that are as large as those for BQ$^{\bullet-}$, and the former point is responsible for the fact that Δg_{yy} for ubisemiquinones is the largest of all systems studied here.

Figure 10 compares the Δg_{yy} values computed for Q$^{\bullet-}$(H$_2$O)$_4$ and Q$^{\bullet-}$(*i*PrOH)$_4$ models with experimental values. The calculated values are overall slightly too low, and the more elaborate Q$^{\bullet-}$(*i*PrOH)$_4$ models exhibit slightly worse agreement with experimental values. However, the much smaller range of values covered has to be kept in mind. The deviations are generally in the range of experimental errors, and thus both models may be considered to reproduce the experimental data (cf. Table 5). Extra hydrogen bonding to methoxy substituents in UQ-M$^{\bullet-}$(L)$_6$ models appears to have only a small influence on Δg_{yy} (cf. Table 4).

6. Atomic Analyses of g-Tensor Data

The atomic nature of the AMFI SO operators used allows the straightforward breakdown of the $\Delta\mathbf{g}_{SO/OZ}$ components into atomic contributions, by setting the SO operators to zero for selected atoms or groups of atoms. Table 6 provides the results of such analyses for various BQ$^{\bullet-}$ model systems. As expected,[16,22] and as found previously in the same type of analyses for the related phenoxyl radical,[24] SO coupling at the carbonyl oxygen atoms dominates both $\Delta g_{SO/OZ,xx}$ and $\Delta g_{SO/OZ,yy}$, with nonnegligible additional contributions from C_{ipso} (i.e., the carbonyl carbon atoms), and in particular from the remaining ring carbon atoms. The latter reduce Δg_{xx} and enhance Δg_{yy}. As we move from unsolvated BQ$^{\bullet-}$ to the solvated model BQ$^{\bullet-}$(H$_2$O)$_4$, it becomes obvious that hydrogen bonding reduces mainly the carbonyl oxygen contributions to Δg_{xx}. This may be attributed to a large part to an enhanced energy gap between the HOMO (largely in-plane oxygen lone pairs, which are stabilized by the hydrogen bonds) and the out-of-plane SOMO.[3,6,13,16,22,52,52] Contributions from the water oxygen atom are generally minor.

Interesting details are provided by examining the simpler model BQ$^{\bullet-}$(H$_2$O) (Table 6). The results show that it is the contribution from the directly hydrogen-bonded carbonyl oxygen atom that is reduced drastically, whereas the contribution from the second carbonyl oxygen atom (to both Δg_{xx} and Δg_{yy}) is actually enhanced, due to a redistribution of spin density[44b] within the delocalized semiquinone system. This redistribution may also be seen from the different contributions of the ring carbon atoms to both Δg_{xx} and Δg_{yy}. Upon moving the coordinated water molecule out of the ring plane by $\gamma = 60°$, the contributions from the carbonyl oxygen atoms to Δg_{xx} increase, and their sum approaches almost that in unsolvated BQ$^{\bullet-}$, consistent with the γ-dependence of this component (cf. Figure 4).

Table 7 summarizes atomic contributions for DQ$^{\bullet-}$ models. Comparison of unsolvated DQ$^{\bullet-}$ and BQ$^{\bullet-}$ provides information about the mechanism by which the methyl substituents influence the **g**-tensor. The substituent effects are again mainly due to reduced contributions from the carbonyl oxygen atoms. Interest-

Table 5. Results of Linear Regression Analyses for Δg_{xx} and Δg_{yy} Computed with Different Models in Comparison with Experimental Data[a]

	Δg_{xx}				Δg_{yy}			
model	A	B	R[b]	SD[c]	A	B	R[b]	SD[c]
free $Q^{\bullet-}$	1.483[d]	−77[d]	0.843[d]	310[d]	1.056[d]	0[d]	0.968[d]	44[d]
	(1.097[e])	(+1299[e])	(0.590[e])	(493[e])	(1.016[e])	(+112[e])	(0.965[e])	(44[e])
$Q^{\bullet-}(H_2O)_4$	1.137	−34	0.920	159	1.089	−331	0.940	64
with $UQ^{\bullet-}(H_2O)_6$[f]	1.250	−433	0.961	117	1.088	−326	0.940	64
$Q^{\bullet-}(i\text{PrOH})_4$	0.948	+489	0.948	79	1.171	−652	−0.943	67
with $UQ^{\bullet-}(i\text{PrOH})_6$[f]	1.128	−150	0.969	95	1.152	−599	−0.941	67
+ SOS-DFPT correction	1.109	−212	0.929	144	1.168	−662	−0.949	63

[a] $\Delta g_{ii}(\text{calc}) = A\Delta g_{ii}(\text{exp}) + B$. UDFT-BP86 results. [b] Regression coefficient. [c] Standard deviation in ppm. [d] Dihedral angle θ for methoxy groups fixed to 110° for UQ-$M^{\bullet-}$ (filled squares in Figure 6; cf. also Figure 9). [e] Fully optimized structure for UQ-$M^{\bullet-}$, cf. open square in Figure 6. [f] Extra hydrogen bonding to methoxy groups in $UQ^{\bullet-}$ taken into account (cf. solid triangles and solid circles in Figures 6 and 9, respectively).

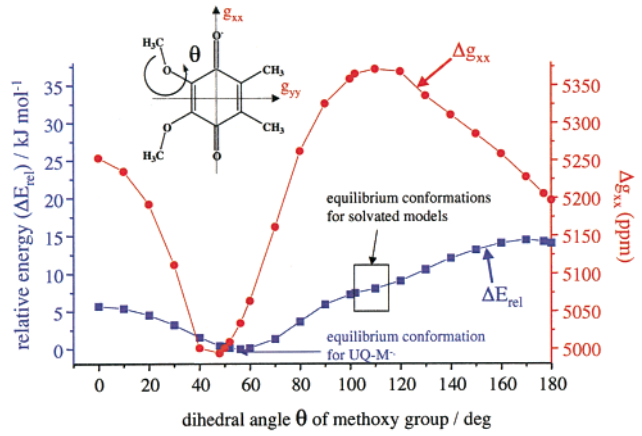

Figure 7. Plot of relative total energy and of Δg_{xx} (UDFT-BP86 results) in UQ-$M^{\bullet-}$ as function of out-of-plane dihedral angle θ for one methoxy group. For each value of θ, all other degrees of freedom have been reoptimized.

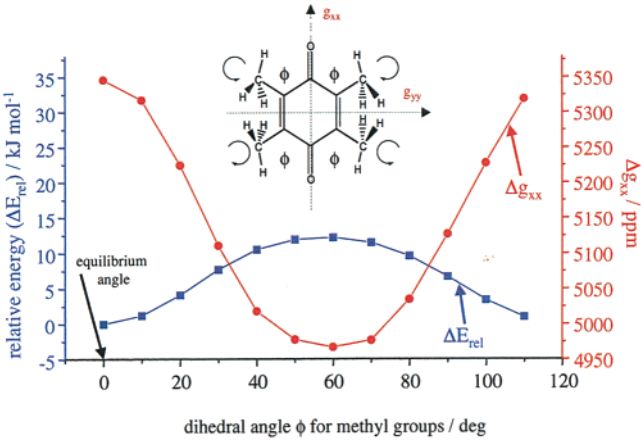

Figure 8. Plot of relative total energy and of Δg_{xx} (UDFT-BP86 results) in $DQ^{\bullet-}$ as function of methyl-group out-of-plane dihedral angle ϕ. The rotation follows the lowest-energy methyl-group rotation mode (A_{2u} symmetry) obtained from harmonic vibrational frequency analysis at the D_{2h} symmetrical minimum structure. For each value of ϕ, all other degrees of freedom have been reoptimized within the constraints of D_2 symmetry.

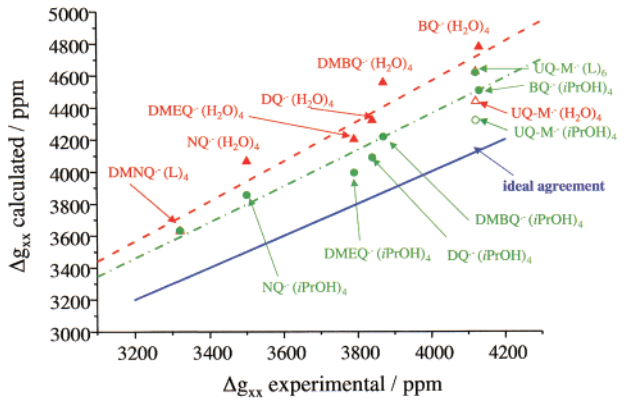

Figure 9. Plot of computed vs experimental Δg_{xx} (UDFT-BP86 results). Model complexes with water molecules (dashed regression; filled triangles) and with 2-propanol molecules (dash−dotted regression line; filled circles) are compared. Extra data points given for UQ-$M^{\bullet-}(H_2O)_4$ (open triangle) and for UQ-$M^{\bullet-}(i\text{PrOH})_4$ (open circle). The solid line represents ideal correspondence between calculation and experiment.

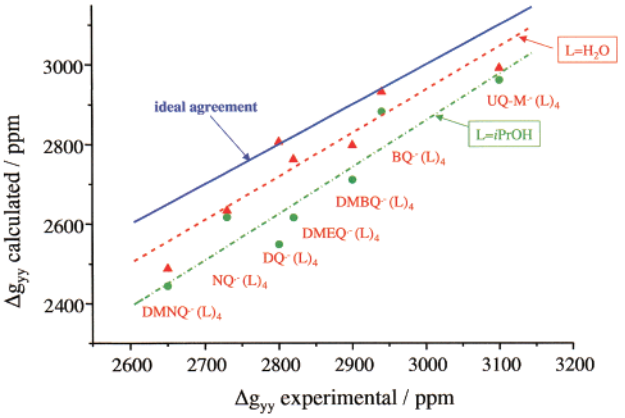

Figure 10. Plot of computed vs experimental Δg_{yy} (UDFT-BP86 results). Model complexes with four water molecules (dashed regression line; filled triangles) and with four 2-propanol molecules (dash−dotted regression line; filled circles) are compared. The solid line represents ideal correspondence between calculation and experiment.

ingly, the negative contributions of the ring carbon atoms to Δg_{xx} are enhanced in $DQ^{\bullet-}$ compared to $BQ^{\bullet-}$ and thus also contribute to the "high-field shift" found for the substituted system. This is consistent with the idea that the methyl substituents influence the **g**-tensor mainly by withdrawing spin density from the carbonyl oxygen atoms and placing it[44] on the ring carbon atoms. Rotation of the methyl substituents into a conformation where the in-plane hydrogen atoms face each other ($\phi = 60°$) reduces the contributions from the carbonyl oxygen atoms to Δg_{xx} even further and thus gives rise to the observed conformational dependence of the **g**-tensor anisotropy (cf. Figure 8). Direct contributions from SO coupling of the methyl carbon atoms are essentially negligible.

Hydrogen bonding in $DQ^{\bullet-}(H_2O)_4$ influences again mainly the contributions from the carbonyl oxygen atoms, but it also modifies the other terms, due to some redistribution of spin density.[44] An interesting side observation is the small but significant negative contribution to Δg_{zz} from the water oxygen atoms, which contrasts to the similarly small but positive

Table 6. Breakdown of $\Delta g_{SO/OZ,uv}$ into Atomic Contributions (in ppm) for Different $BQ^{\bullet-}$ Model Systems[a]

	atom(s)	Δg_{xx}	Δg_{yy}	Δg_{zz}
$BQ^{\bullet-}$ unsolvated	2xO(CO)	6669.9	2520.0	−16.7
	$2xC_{ipso}$	−78.9	48.7	2.4
	$4xC_{ring}$	−277.5	409.5	1.9
	Σ	6313.5	2978.2	−12.4
	total	*6313.6*	*2978.1*	*−12.5*
$BQ^{\bullet-}(H_2O)_4$	2xO(CO)	5110.7	2443.7	1.4
	$2xC_{ipso}$	−39.8	32.7	0.9
	$4xC_{ring}$	−236.9	402.2	−2.2
	$4xO(H_2O)$	−24.0	−7.5	23.6
	Σ	4809.8	2871.0	23.6
	total	*4809.9*	*2864.0*	*30.8*
$BQ^{\bullet-}(H_2O)$ opt.[b,d]	O(CO···H)	2644.0	1182.8	−1.8
	O(CO)	3689.0	1327.8	−10.4
	C1	−29.4	31.3	−0.3
	C1′	−38.2	15.8	2.2
	C2	−71.6	79.1	−0.1
	C2′	−61.0	95.5	0.0
	C3	−92.1	136.9	0.4
	C3′	−94.0	145.7	0.4
	$O(H_2O)$	−9.3	−5.5	14.1
	Σ	5937.3	3005.3	4.4
	total	*5984.6*	*2964.0*	*2.5*
$BQ^{\bullet-}(H_2O)$ 60^0 [c,d]	O(CO···H)	2904.5	1163.1	−7.2
	O(CO)	3657.2	1320.7	−10.1
	C1	−27.1	56.8	−2.3
	C1′	−37.4	17.6	1.0
	C2	−81.4	87.1	−0.7
	C2′	−74.3	93.4	−1.0
	C3	−88.9	133.4	−0.7
	C3′	−37.4	17.6	1.0
	$O(H_2O)$	−14.2	126.5	21.9
	Σ	6200.9	3016.1	2.5
	total	*6206.9*	*3025.9*	*51.5*

[a] UDFT results. Atomic contributions have been computed by setting the AMFI−SO operators to zero for all other atoms. Contributions from hydrogen atoms are generally negligible. Small deviations of the sum of all contributions from the total value result from slight differences in the orientation of the principal axes system for calculations with truncated SO operators. [b] Fully optimized structure. [c] Structure with γ fixed to 60° (cf. Figure 4). [d] Cf. Figure 4 for atom labels.

contribution in $BQ^{\bullet-}(H_2O)_4$ (cf. Table 6). These differences are related to the out-of-plane orientation of the hydrogen bonds in the durosemiquinone system, which also results in changes of the hyperfine interactions with the coordinated solvent molecules.[44]

The same types of analyses are shown in Table 8 for the unsolvated UQ-$M^{\bullet-}$ model system. The most notable difference relative to $BQ^{\bullet-}$ is again the significantly reduced carbonyl oxygen contribution to Δg_{xx}. Interestingly, the methoxy oxygen atoms contribute ca. +138 ppm to Δg_{yy}. This explains why the ubiquinone systems exhibit larger Δg_{yy} components than any of the other semiquinones studied, including the parent $BQ^{\bullet-}$. Rotating the methoxy substituents from the optimum $\theta = 56.2°$ for the unsolvated system to $\theta = 110°$ typical for the solvated systems mainly enhances the carbonyl oxygen contribution to Δg_{xx}. While the other contributions are also modified, the analysis does not allow an unambiguous interpretation. We suspect, however, that changes in the repulsive interactions between the methoxy oxygen lone pairs and the π-type SOMO of the semiquinone are responsible for the unexpectedly pronounced conformational effects on Δg_{xx}.

7. Discussion, Relevance to EPR of Semiquinone Radical Anions in Proteins

To reproduce experimental Δg_{xx} values of semiquinone radical anions in 2-propanol solution, we had to properly account for hydrogen bonding from the solvent to the carbonyl oxygen atoms, as well as for the conformational preferences of the substituents of the quinone system. We find the latter to be inherently coupled to the orientation of the hydrogen bonds, with very little energy needed to cooperatively change the structure to another arrangement. A proper treatment of the resulting dynamical contributions to the **g**-shifts would require a combination of the present DFT **g**-tensor calculations with molecular dynamics simulations. This is beyond the scope of the present study. Apart from the systematic DFT errors (see below), the neglect of the substituent and solvent dynamics is

Table 7. Breakdown of $\Delta g_{SO/OZ,uv}$ into Atomic Contributions (in ppm) for Different $DQ^{\bullet-}$ Model Systems[a]

	atom(s)	Δg_{xx}	Δg_{yy}	Δg_{zz}
$DQ^{\bullet-}$ unsolvated fully optimized	2xO(CO)	5915.4	2488.9	−14.8
	$2xC_{ipso}$	−119.1	30.8	0.4
	$4xC_{ring}$	−394.5	368.8	−4.7
	$4xC(CH_3)$	−3.6	3.2	−0.5
	Σ	5398.2	2891.7	−19.6
	total	*5378.8*	*2918.0*	*−20.6*
$DQ^{\bullet-}$ unsolvated $\phi = 60°$ [b]	2xO(CO)	5488.7	2479.7	−16.3
	$2xC_{ipso}$	−128.0	27.9	0.7
	$4xC_{ring}$	−361.1	285.4	−7.4
	$4xC(CH_3)$	−13.1	−1.4	1.0
	Σ	4986.5	2791.6	−22.0
	total	*5000.4*	*2780.1*	*−24.5*
$DQ^{\bullet-}(H_2O)_4$	2xO(CO)	4766.4	2236.4	−7.2
	$2xC_{ipso}$	−79.5	12.0	−0.7
	$4xC_{ring}$	−284.4	373.1	−4.6
	$4xC(CH_3)$	−0.5	9.2	−1.6
	$4xO(H_2O)$	−36.9	−26.7	−47.3
	Σ	4365.1	2604.0	−61.4
	total	*4363.5*	*2605.3*	*−61.7*

[a] UDFT results. Contributions of atoms or groups of atoms have been computed by setting the AMFI−SO operators to zero for all other atoms. Contributions from hydrogen atoms are generally negligible. Small deviations of the sum of all contributions from the total value result from slight differences in the orientation of the principal axes system for calculations with truncated SO operators. [b] Structure with ϕ fixed to 60° (cf. Figure 9).

Table 8. Breakdown of $\Delta g_{SO/OZ,uv}$ into Atomic Contributions (in ppm) for UQ-$M^{\bullet-}$ [a]

	atom(s)	Δg_{xx}	Δg_{yy}	Δg_{zz}
UQ-$M^{\bullet-}$ fully opt.[b]	2xO(CO)	5476.7	2632.7	−17.7
	$2xO(OCH_3)$	10.1	137.6	3.3
	C1+C1′	−135.1	64.2	1.8
	C2,C3[c]	−185.9	171.5	−2.9
	C2′,C3′ [d]	−204.1	134.5	−5.0
	$2xC(CH_3)$	−1.8	2.5	−1.5
	$2xC(OCH_3)$	4.0	1.5	26.8
	Σ	4963.9	3144.5	−7.0
	total	*5059.3*	*3144.4*	*−90.7*
UQ-$M^{\bullet-}$ OCH_3 groups at $\theta = 110^0$ [b]	2xO(CO)	6277.1	2608.0	−22.3
	$2xO(OCH_3)$	−3.0	162.1	−3.1
	C1+C1′	−112.1	51.1	1.5
	C2,C3[c]	−203.3	170.0	−2.3
	C2′,C3′ [d]	−236.6	167.9	−2.2
	$2xC(CH_3)$	−3.9	2.2	−0.3
	$2xC(OCH_3)$	−8.3	−1.9	−2.4
	Σ	5709.9	3159.4	−31.1
	total	*5706.3*	*3159.5*	*−27.8*

[a] UDFT results. Contributions of atoms or groups of atoms have been computed by setting the AMFI−SO operators to zero for all other atoms. Contributions from hydrogen atoms are generally negligible. Small deviations of the sum of all contributions from the total value result from slight differences in the orientation of the principal axes system for calculations with truncated SO operators. [b] cf. Figure 2b for the definition of θ and for atom labels. [c] Neighboring CH_3 substituents. [d] Neighboring OCH_3 substituents.

thus probably responsible for the largest part of the remaining uncertainties in our comparison with experimental values.

However, using our best $Q^{\bullet-}(i\text{PrOH})_4$ computational models [including the UQ-$M^{\bullet-}(i\text{PrOH})_6$ values] and gradient-corrected density functionals, even the present static calculations provide remarkable agreement with experimental values, with a systematic overestimate of the range of Δg_{xx} values by ca. 10% (cf. Table 5). Similar accuracy, and the same overestimate of the range of tensor values, has been found in many previous applications of closely related DFT approaches to NMR chemical shifts of main group compounds[28,43,53] or of main-group nuclei in transition metal complexes.[54] The systematic overestimate of the paramagnetic contributions is thought to be due to deficiencies in the present state-of-the-art density functionals. The observed magnitude of deviation is as expected if no significant errors arise from other sources, e.g., from the SO operators (cf. section 2). Thus, we may expect that improved functionals will perform even better. Indeed, preliminary test calculations with newly implemented meta-GGA functionals provide ca. 5% lower $\Delta\mathbf{g}_{SO/OZ}$ contributions.[55] Relatively straightforward ways may be used to semiempirically correct the results for the systematic DFT errors. One possible way to reduce $\Delta\mathbf{g}_{SO/OZ}$ is to include the SOS-DFPT correction terms, but the slightly improved slope of the regression lines for Δg_{xx} is accompanied by a somewhat worse correlation (Table 5). However, already a simple scaling of the computed Δg_{xx} values by 0.92 reduces all individual absolute deviations from experiment to below 130 ppm. As the reported experimental uncertainty is probably on the order of ca. $\pm$100 ppm,[6] this means that the scaled values agree generally to within experimental accuracy. As solvent and conformational effects appear to be less important for Δg_{yy}, in this case even the simplest unsolvated models come to within experimental accuracy.

Thus, at the present level of accuracy, DFT methods should already be useful to make predictions for experimentally less well studied cases. Notably, comparison of the Δg_{xx} and Δg_{yy} values computed with solvated and unsolvated model systems should provide a good quantitative estimate of the influence of hydrogen bonding on the **g**-shifts. In fact, the unsolvated and solvated models are expected to give upper and lower bounds, respectively, of the values to be found at intermediate hydrogen bonding strength as considered, e.g., for the radical anion of Vit-K_1 ($A^{\bullet-}$) in native PS$-$I. Only few **g**-tensors of semiquinones have been determined in aprotic solvents. Two cases, $DQ^{\bullet-}$ in 2-methyltetrahydrofuran (MTHF)[6] and UQ-$3^{\bullet-}$ in DME/MTHF mixtures (DME = dimethoxyethane),[7] are included in Table 4. In the case of $DQ^{\bullet-}$, Δg_{xx} in 2-propanol is reduced by ca. 600 ppm compared to the data in MTHF. The computational results for unsolvated and solvated models indicate a larger reduction by more than 1000 ppm (Table 4). Comparison of our results for the UQ-$M^{\bullet-}$ model with data for UQ-$3^{\bullet-}$ in DME/MTHF mixtures[7] is complicated by the question of methoxy group conformation. Depending on whether the optimized conformation or the $\theta = 110°$ conformation is presumed for the unsolvated radical (Table 4), the computed reduction of Δg_{xx} by hydrogen bonding is either smaller or larger than the difference between aprotic and protic solvent data. We note that in all cases studied computationally, *both* Δg_{xx} *and* Δg_{yy} are reduced by hydrogen bonding (Table 4). It appears possible that other solvent effects than hydrogen bonding may affect the **g**-shift components in ether solution, and thus the comparison with the isolated radicals is not fully warranted. An earlier comparison of isotropic *g*-values of $BQ^{\bullet-}$ in liquid water and in dimethyl sulfoxide gave a relatively large reduction of Δg_{iso} from 3200 to 2400 ppm,[16] in good agreement with the computed difference between $BQ^{\bullet-}$ and $BQ^{\bullet-}(i\text{PrOH})_4$ (Table 4). Larger differences between DME/MTHF and 2-propanol solvents than for UQ-$3^{\bullet-}$ have been found for UQ-$0^{\bullet-}$ (which has a hydrogen atom instead of the side chain in 3-position).[7]

In photosynthetic reaction centers and other enzymes that contain quinones, the protein environment influences not only the EPR parameters of semiquinone radical anions but also their redox potential, and thus the biological function of the different types of reaction centers (see Introduction). The study of these interactions is thus central to understanding biological function. The robustness of the present DFT approach should allow comparisons also with experimental **g**-tensor data obtained in protein environment. Table 4 includes experimental data for $DQ^{\bullet-}$ and $NQ^{\bullet-}$ not only in frozen 2-propanol solution but also as measured in zinc-substituted bacterial reaction centers (Zn-bRC) and in PS$-$I, into which these quinones had been reconstituted.[9] The **g**-shift components of the two semiquinone radical anions in the Q_A site of Zn-bRC are very close to those in isotropic solution. This has been taken as an indication for relatively strong hydrogen bonding.[9] In contrast, the Δg_{xx} values measured for the two radicals in PS$-$I are much closer (probably too close) to the data computed for unsolvated systems (4920 and 5030 ppm for $DQ^{\bullet-}$ and $NQ^{\bullet-}$, respectively, after scaling by 0.92). However, the more interesting comparison in this case pertains to the very large Δg_{yy} values measured for both radical anions in PS$-$I. In both cases, these Δg_{yy} components are ca. 1000 ppm larger than even the computational results for the unsolvated models. Hydrogen bonding reduces Δg_{yy} (cf. Table 4), and neither conformational substituent effects nor systematic DFT errors can account for a discrepancy of this magnitude. Therefore, it appears that the very large Δg_{xx} *and* Δg_{yy} values found for $DQ^{\bullet-}$ and $NQ^{\bullet-}$ substituted into PS$-$I may indicate further interactions with the protein environment (other than hydrogen bonding to the carbonyl oxygen atoms) that have not yet been accounted for. Possible candidates are interactions with nearby tryptophan residues, which are however known to be located near the active sites in both bRCs *and* PS$-$I.[10,12] Interestingly, the Δg_{yy} values measured for native Vit-$K_1^{\bullet-}$ in PS$-$I ($A^{\bullet-}$; cf. Table 4) differ less from those found in frozen 2-propanol, even though the Δg_{xx} components are increased, i.e., the very large Δg_{yy} values appear to be restricted to the case of the smaller $DQ^{\bullet-}$ and $NQ^{\bullet-}$ radicals. After submission of the initial version of this manuscript, the X-ray structure analysis of PS$-$I of *S. elongatus* at 2.5 Å resolution has been reported.[56] It confirms in both possible A_1 sites (i) one hydrogen

(53) Schreckenbach, G.; Ziegler, T. *Theor. Chem. Acc.* **1998**, *2*, 71. Bühl, M.; Kaupp, M.; Malkin, V. G.; Malkina, O. L. *J. Comput. Chem.* **1999**, *20*, 91.
(54) Kaupp, M.; Malkina, O. L.; Malkin, V. G. in: *Encyclopedia of Computational Chemistry*; Schleyer, P. v. R., Ed.; Wiley-Interscience, New York, 1998; pp 1857−1866.
(55) For example, calculations with the new program system ReSpect[42] and the PKZB meta-GGA functional (Perdew, J. P.; Kurth, S.; Zupan, A.; Blaha, B. *Phys. Rev. Lett.* **1999**, *82*, 2544) gave the following results for $BQ^{\bullet-}$: Δg_{xx} = 5946 ppm, Δg_{yy} = 2950 ppm, Δg_{zz} = 21 ppm. This should be compared to the GGA (BP86) results obtained with the same implementation: Δg_{xx} = 6238 ppm, Δg_{yy} = 3057 ppm, Δg_{zz} = 21 ppm (Arbouznikov, A.; Kaupp, M.; Malkina, O. L.; Malkin, V. G., unpublished results).
(56) Jordan, P.; Fromme, P.; Witt, H. T.; Klukas, O.; Saenger, W.; Krauss, N. *Science* **2001**, *411*, 909.

bond to a carbonyl oxygen of the quinone (Vit-K_1) and (ii) π-stacking between a tryptophan residue and the quinone. We are presently carrying out further calculations to study the influence of these interactions on the **g**-tensors of semiquinone radical anions.[57]

8. Conclusions

The present systematic computational study of a series of semiquinone radical anions has confirmed that the use of density functional theory, combined with accurate approximations to the full spin−orbit operators,[24] allows quantitative calculations of **g**-tensors for organic radicals. After accounting for the influences of hydrogen bonding and of substituent conformation, the calculations have reproduced the experimentally observed substituent effects in detail. For example, peculiar effects of the conformation of the methoxy groups in ubisemiquinone systems on spin density distribution and **g**-shifts have been demonstrated. Calculations on realistic solvated model systems have provided quantitative estimates of the influence of hydrogen bonding on the **g**-tensors. The atomic nature of the one-center meanfield spin−orbit operators has furthermore allowed the detailed analysis of the computed tensors in terms of atomic contributions.

As for other properties, the particular attraction of the DFT approach to electronic **g**-tensors arises from the combination of accuracy and computational efficiency. For example, in the present study, we have included many hydrogen-bonded complexes with up to ca. 100 atoms (indeed, the computational bottleneck has been the DFT structure optimization, not the **g**-tensor calculation). The remaining overestimate of the $\Delta g_{SO/OZ}$ contribution by present-day density functionals on the order of ca. 10% appears to be reasonably systematic and is comparable to observations made earlier for density functional calculations of NMR chemical shifts. As in the NMR case, these errors may be corrected for straightforwardly, e.g., by simple scaling. Moreover, improved density functionals are expected to provide even better results in the future. In the previous section, we have already shown an example in which DFT calculations enabled us to point out some pecularities of **g**-tensors measured for semiquinone radical anions in different protein environments. We may expect useful applications of the present DFT approach in many other areas. In the case of bioradicals, further studies are presently being carried out for tyrosyl radicals,[58] and for nitroxide spin labels.[59] However, the accuracy found for the approach in this and the previous[24] study indicates that we may also make useful predictions for radicals that have not yet been studied experimentally at all.

Acknowledgment. M.K. is grateful to Dr. F. MacMillan (Frankfurt) for helpful comments on the manuscript. This study has been supported by Deutsche Forschungsgemeinschaft (Priority Program SP1051, "High-Field EPR") and by Fonds der Chemischen Industrie. Part of this work benefitted also from the graduate college "Moderne Methoden der magnetischen Resonanz in der Materialforschung" at Universität Stuttgart. J.V. is on leave from the NMR Research Group, Department of Physical Sciences, University of Oulu, Finland, and has been supported by the Academy of Finland (Grant 48578) and by the Magnus Ehrnrooth Fund of the Finnish Society of Sciences and Letters. Financial support from the Slovak Grant Agency VEGA (Grant ~2/4012/01) is gratefully acknowledged by V.G.M. and O.L.M.

Supporting Information Available: Two figures with conformational profiles of Δg_{yy} of $DQ^{\bullet-}$ and UQ-$M^{\bullet-}$ and tables with cartesian coordinates of all molecules studied. This material is available free of charge via the Internet at http://pubs.acs.org.

JA0162764

(57) Kaupp, M. *Biochemistry*, in press.

(58) Kaupp, M., unpublished results.

(59) Engström, M., *Ph.D. Thesis*, University of Linköping, Sweden 2001.